Origin and evolution of the Kangâmiut mafic dyke swarm, West Greenland

Kyle R. Mayborn and Charles E. Lesher

The Kangâmiut dyke swarm in West Greenland intruded Archaean terrains at 2.04 Ga, and its northern portion was subsequently metamorphosed to granulite facies during the Nagssugtoqidian orogeny (*c*. 1.8 Ga). Mineral and whole-rock major and trace element compositions show that the parental magmas for the dyke swarm differentiated by the fractionation of olivine, clinopyroxene, plagioclase and late stage Fe-Ti oxides. Petrographical observations and the enrichment of K_2O during differentiation argue that hornblende was not an important fractionating phase. Field observations suggest emplacement at crustal levels above the brittle–ductile transition, and clinopyroxene geothermobarometry constrains dyke emplacement depths to less than 10 km. Granulite facies metamorphism of the Kangâmiut dykes and their host rocks in the northern portion of the swarm requires subsequent burial to *c*. 30 km, related to roughly 20 km of crustal thickening between the time of dyke emplacement and peak metamorphism during the Nagssugtoqidian orogeny. Kangâmiut dykes are characterised by low Ba/La ratios (12 ± 5), and high Nb/La ratios (0.8 ± 0.2), compared to subduction related basalts (Ba/La *c*. 25; Nb/La *c*. 0.35). These geochemical characteristics argue that the Kangâmiut dykes are not related to subduction processes. Forward modelling of rare-earth element data requires that primitive magmas for the Kangâmiut dykes originated from a moderately depleted mantle source with a mantle potential temperature of *c*. 1420°C. The inferred potential temperature is consistent with potential temperature estimates for ambient mantle at 2.0 Ga derived from secular cooling models and continental freeboard constraints. The geochemistry and petrology of the Kangâmiut dykes support a model that relates the dyke activity to passive rifting of the proposed Kenorland supercontinent rather than to mantle plume activity or subduction.

Keywords: dyke swarm, Laurentia, Palaeoproterozoic, rifting

K.R.M., *Department of Geology, Western Illinois University, Macomb, IL 61455, USA.* E-mail: *KR-Mayborn@wiu.edu*
C.E.L., *Department of Geology, University of California-Davis, Davis, CA 95616, USA.*

The 2.04 Ga Kangâmiut dyke swarm of West Greenland has been the subject of numerous investigations over the past 35 years (Windley 1970; Escher *et al.* 1976; Bridgwater *et al.* 1995; Cadman *et al.* 1999), yet there is still considerable disagreement over many aspects of the swarm's history. Since the work of Escher *et al.* (1976), who associated the dykes with synkinematic shearing during N–S compression, the swarm has often been cited as a type example of dykes that are emplaced into crustal regions undergoing shear deformation (Cadman *et al.* 1999). The proposed compressional setting led Cadman *et al.* (2001) to speculate that the swarm formed in a subduction-related environment. Nevertheless, recent geochronology has shown that many of the shear zones originally thought to be consanguineous with the dykes are actually significantly older or younger than the dykes themselves (Connelly & Mengel 2000). The field area for Escher *et al.*'s (1976) investigations is now known to contain Archaean shear

zones and post-Kangâmiut dyke shearing associated with the Nagssugtoqidian orogeny. Despite these complications, the Kangâmiut dyke swarm offers a unique opportunity to constrain the magmatic and tectonic evolution of the province spanning the period from dyke emplacement to the Nagssugtoqidian orogeny (2.04 to *c.* 1.8 Ga). The present work discusses the constraints on the magmatic and metamorphic history of the Kangâmiut dykes provided by field observations, petrology, geochemistry, and geochronology and critically evaluates previous and newly proposed models for their origin and subsequent metamorphism during the Nagssugtoqidian orogeny.

Regional geology

Figure 1 is a geological map of central West Greenland showing the Nagssugtoqidian orogen and the Kangâmiut dykes. The Nagssugtoqidian orogen is bounded to the north by the Palaeoproterozoic Rinkian orogen (Escher & Pulvertaft 1976) and to the south by the Archaean Nain craton (Nutman & Bridgwater 1986; Nutman & Collerson 1991; Friend & Nutman 1994). The orogen is divided into four parts based on lithology, structure, stream sediment geochemistry, and aeromagnetic data. From north to south, these are the northern Nagssugtoqidian orogen (NNO), the central Nagssugtoqidian orogen (CNO), the southern Nagssugtoqidian orogen (SNO), and the southern Nagssugtoqidian foreland (SNF). These terrains are separated by three shear zones. The Nordre Strømfjord shear zone separates the NNO from the CNO, the Ikertôq shear zone separates the CNO from the SNO, and the Nagssugtoqidian Front separates the SNO from the SNF.

The NNO contains Archaean granitic gneisses and supracrustal rocks (van Gool *et al.* 2002), whereas the CNO is characterised by reworked Archaean granitic and tonalitic gneisses, the 1.92 Ga Arfersiorfik quartz diorite, the 1.92 Ga Sisimiut charnockite, and supracrustal rocks (Bak *et al.* 1975; Kalsbeek *et al.* 1987; Manatschal *et al.* 1998; Kalsbeek & Manatschal 1999; Nutman *et al.* 1999; van Gool *et al.* 1999). The SNO and SNF are composed of Archaean granitic and tonalitic gneisses and the Kangâmiut dykes. In the SNO the dykes are metamorphosed to amphibolite facies in the south and granulite facies in the extreme north. The transition from amphibolite facies to granulite facies occurs within the Ikertôq shear zone (Korstgård 1979). In the SNF, most of the Kangâmiut dykes retain igneous textures and mineralogies.

Figure 1 shows that the Ikertôq shear zone is the most continuous structure within the Nagssugtoqidian orogenic belt and represents an important lithological boundary between the SNO and the CNO. It is traceable from the western shoreline, just south of the village of Sisimiut, to the inland icecap. The shear zone contains panels of Kangâmiut dyke-bearing tonalitic gneiss alternating with layers of garnet-sillimanite-kyanite-bearing metapelites, marbles, and quartzites that dip steeply NNW. The repetition of lithological units, the presence of down-dip lineations and S-vergent kinematic indicators show that this structure is a reverse fault (Grocott 1979). Deformed Kangâmiut dykes are restricted to the southern footwall, while Palaeoproterozoic felsic igneous rocks, including the 1.92 Ga Sisimiut charnockite and the 1.92 Ga Arfersiorfik quartz diorite, are found only north of the shear zone. U/Pb dates for detrital zircons from the supracrustal rocks of the region require that these units were deposited after 2.10 Ga (Nutman *et al.* 1999), while $^{40}Ar/^{39}Ar$ dating of hornblende from metamorphosed Kangâmiut dykes and orthogneisses from within the shear zone gives cooling ages of *c.* 1.73 Ga (Willigers *et al.* 1999).

The Itivdleq shear zone is located to the south of the Ikertôq shear zone within the SNO and is *c.* 6 km wide with E–W-trending lineations (Hanmer *et al.* 1997). It contains multiple bands of sheared Kangâmiut dykes and Archaean orthogneisses that Connelly & Mengel (2000) used to document shearing during the Archaean and the Palaeoproterozoic Nagssugtoqidian orogeny. For example, some of the shear bands are cut by weakly deformed tonalites that yield a magmatic age of 2498 ± 4 Ma with a metamorphic overprint at 1782 ± 12 Ma (Connelly & Mengel 2000). This shows that some of the shear bands near Itilleq fjord developed prior to *c.* 2.5 Ga and were subsequently intruded by tonalite. The metamorphic overprint age of 1782 Ma and the presence of shear bands that cut the Kangâmiut dykes indicate reactivation during the Nagssugtoqidian orogeny. Metamorphic hornblende from a recrystallised Kangâmiut dyke within the Itivdleq shear zone gives an $^{40}Ar/^{39}Ar$ age of 1873 ± 13 Ma, consistent with the age of Nagssugtoqidian metamorphism (Willigers *et al.* 1999).

The Nagssugtoqidian Front is the southernmost structural expression of the Nagssugtoqidian orogenic event (Fig. 1). Hageskov (1995) showed that it is a discontinuous, en échelon array of NW-dipping, low-angle thrust

Facing page:
Fig. 1. Geological map of the Nagssugtoqidian orogen and its southern foreland in West Greenland. NNO, northern Nagssugtoqidian orogen; CNO, central Nagssugtoqidian orogen; SNO, southern Nagssugtoqidian orogen; SNF, southern Nagssugtoqidian foreland. Modified from van Gool *et al.* (2002).

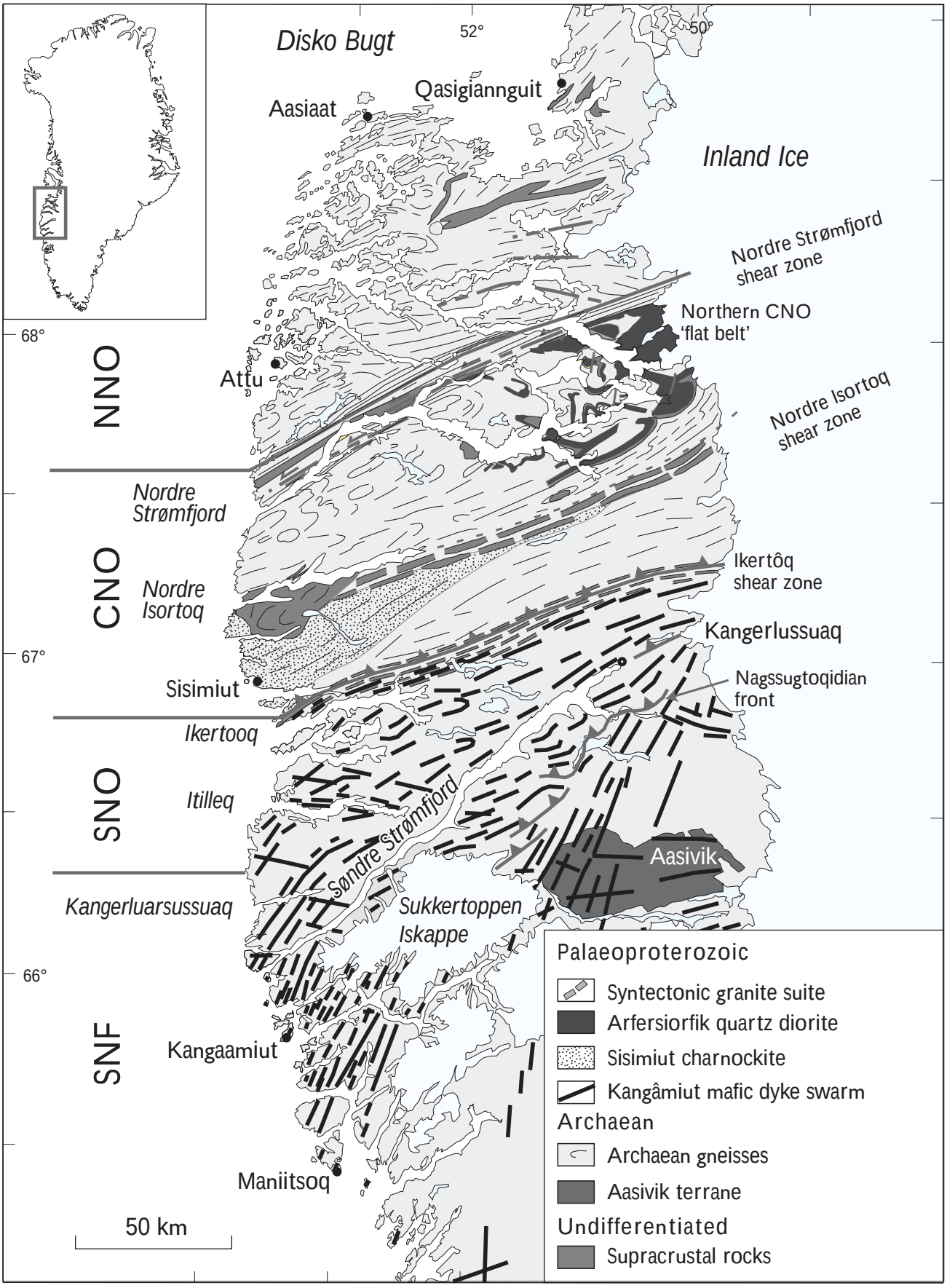
Disko Bugt
52°
50°
Qasigiannguit
Aasiaat
Inland Ice
Nordre Strømfjord shear zone
Northern CNO 'flat belt'
68°
Attu
NNO
Nordre Isortoq shear zone
Nordre Strømfjord
CNO
Nordre Isortoq
Ikertôq shear zone
Kangerlussuaq
67°
Sisimiut
Nagssugtoqidian front
Ikertooq
SNO
Itilleq
Søndre Strømfjord
Aasivik
Kangerluarsussuaq
Sukkertoppen Iskappe
66°
SNF
Kangaamiut
Maniitsoq
50 km
Palaeoproterozoic
Syntectonic granite suite
Arfersiorfik quartz diorite
Sisimiut charnockite
Kangâmiut mafic dyke swarm
Archaean
Archaean gneisses
Aasivik terrane
Undifferentiated
Supracrustal rocks

faults that deformed the Kangâmiut dykes in this region. The Nagssugtoqidian Front is well defined in the eastern portion of the orogen but is difficult to trace to the west approaching the Sukkertoppen Iskappe. It is not known whether the Nagssugtoqidian Front dies out beneath the icecap or swings to the NNW merging with the Itivdleq shear zone (Hageskov 1995).

Geological history

The Precambrian history of central West Greenland involves five major events: (1) genesis and metamorphism of Archaean crust; (2) emplacement of the Kangâmiut dykes (2.04 Ga); (3) deposition of sediments (*c*. 2.00–1.92 Ga); (4) emplacement of the Sisimiut and Arfersiorfik intrusions (*c*. 1.92–1.87 Ga); and (5) metamorphism and deformation accompanying the Nagssugtoqidian orogeny (*c.* 1.82–1.77 Ga).

Genesis and metamorphism of Archaean crust

Connelly & Mengel (2000) and Kalsbeek & Nutman (1996) present U/Pb dates and field observations that document the genesis and metamorphism of a large portion of the central West Greenland crust during the Late Archaean. Igneous zircons from foliated granulite facies gneisses give ages between 2.87 and 2.81 Ga. Granitoids that cut the foliation in these gneisses give ages between 2.81 and 2.72 Ga. These cross-cutting relationships and dates indicate widespread genesis of granitic crust between 2.87 and 2.81 Ga, immediately followed by metamorphism at 2.81–2.72 Ga.

Emplacement of the Kangâmiut dykes

The emplacement of the Kangâmiut dykes occurred after the formation of the Archaean host rocks and before the Nagssugtoqidian orogeny. U/Pb geochronology on igneous zircons from three dykes gives ages of 2036 ± 5 Ma, 2046 ± 8 Ma (Nutman *et al.* 1999), and 2048 ± 4 Ma (Connelly *et al.* 2000). The analysed zircons come from dioritic centres in wide composite dykes and cover most of the N–S extent of the dyke swarm. $^{40}Ar/^{39}Ar$ dating of hornblende from the Kangâmiut dykes from the SNF by Willigers *et al.* (1999) gives emplacement related ages of 2.05–2.02 Ga.

Deposition of sediments

Dating of detrital zircons from metasedimentary units just south of the Nordre Strømfjord shear zone and within the Ikertôq shear zone (Fig. 1) yields ages between 3.4 and 1.95 Ga (Nutman *et al.* 1999). Some metasediments containing 1.95 Ga zircons are cut by 1.92 Ga quartz-diorites, requiring that deposition of the sediments occurred between 1.95 and 1.92 Ga. Metasediments found within thrust-bounded panels in the Ikertôq shear zone contain zircons that yield ages between 2.1 and 2.0 Ga. There are no known granitic intrusive rocks with ages between 2.5 and 1.92 Ga within the central West Greenland field area, suggesting that the sediments originated from a distal source. Nutman *et al.* (1999) propose that the Archaean and Palaeoproterozoic terranes of eastern Canada are possible source regions. Sediments derived from these terranes would support the existence of the supercontinent Kenorland (Williams *et al.* 1991; Aspler & Chiarenzelli 1998). Additionally, the deposition of sediments suggests the presence of basins that may have developed during the rifting and break-up of Kenorland (van Gool *et al.* 2002).

The Nagssugtoqidian orogeny and emplacement of Sisimiut and Arfersiorfik intrusions

Ramberg (1949) and Noe-Nygaard (1952) first recognised the Nagssugtoqidian orogen based on the deformation and metamorphism of the Kangâmiut dykes and the occurrence of shear zones with steeply dipping foliations. Geochronological data show that the Nagssugtoqidian orogenic event occurred between 1.91 and 1.77 Ga (Connelly *et al.* 2000) and resulted in granulite to amphibolite grade metamorphism and the development of discrete shear zones. Pre-orogenic magmatism includes the emplacement of the 1.92 Ga Arfersiorfik quartz diorite (Kalsbeek *et al.* 1987) and the 1.92 Ga Sisimiut charnockite. The orogenic event is proposed to be the result of continental collision that produced thrust stacking, folding and associated metamorphism (van Gool *et al.* 2002). The suture between the two continents is not easily identifiable, but Kalsbeek *et al.* (1987) proposed that the suture is located in what is now the boundary between the NNO and the CNO.

Previous work on the origin of the Kangâmiut dykes

Many early workers suggested that the emplacement of the Kangâmiut dykes was directly related to the Nagssugtoqidian orogeny. Escher *et al.* (1976) stated that the dykes were emplaced into conjugate sets of active shear zones during NNW–SSE compression. They based this hypothesis on their observations of conjugate sets of dykes that show a variety of cross-cutting relationships. They, and Hanmer *et al.* (1997), proposed that the emplacement of both dyke sets occurred during shearing. Bridgwater *et al.* (1995) expanded on the Escher *et al.* (1976) hypothesis by proposing that the dykes formed during thrusting of amphibolite facies crust from the north under the granulite facies terrain in the southern Nagssugtoqidian orogen. They invoked this hypothesis because the Kangâmiut dykes contain hornblende suggesting they crystallised from a hydrous magma. Bridgwater *et al.'s* (1995) hypothesis seeks to explain the hydrous nature of the Kangâmiut dyke magmas by placing a hydrous source beneath the granulite facies host rocks. A potential problem with the Escher *et al.* (1976) and Bridgwater *et al.* (1995) hypotheses is that neither easily explains how partial melting of hydrous lower crust would directly produce melt of basaltic composition. If the Escher *et al.* (1976) and Bridgwater *et al.* (1995) hypotheses of dyke emplacement during compression are correct, then subduction related magmatism becomes a possibility. Cadman *et al.* (2001) explicitly consider this possibility and proposed that the Kangâmiut dyke swarm formed by adiabatic decompression of metasomatised mantle during passage of a slab window.

The recent work of Kalsbeek & Manatschal (1999), Connelly & Mengel (2000) and van Gool *et al.* (2002), offer alternatives to the subduction hypothesis and suggest that the swarm was emplaced during continental rifting. Van Gool *et al.* (2002) cite evidence of 2.0 Ga rift related sediments in support for the rifting hypothesis. Kalsbeek & Manatschal (1999) speculate that the Kangâmiut dykes are the product of mantle plume-related rifting based on the presence of ultramafic rocks found within the Nagssugtoqidian orogeny. Although these authors discuss the origin of the Kangâmiut dykes, they do so only briefly, because their primary focus is on the Nagssugtoqidian orogeny.

Field setting

The Kangâmiut dyke swarm intruded granulite facies Archaean orthogneisses and is exposed over an 18 000 km^2 area. Figure 1 shows that the swarm extends for 150 km from just south of the village of Maniitsoq towards Sisimiut in the north and from the coast eastward to the ice cap. The dykes are most abundant near the coast and less so towards the ice cap. Dyke widths range from a few centimetres to greater than 140 m. Escher *et al.* (1975) estimated that dyke emplacement was accommodated by 2–3% crustal extension. Appendix A provides locality and field characteristics of all the dykes examined in this study.

Field observations show that there are three dyke suites (Mengel *et al.* 1996). Two of these trend east–west, while the third has a NE trend. The NE-trending suite of dykes represents the vast majority of the dykes in the area and is the only suite that contains dykes with dioritic centres. The three sets of zircon populations used to date three separate dykes all come from these dioritic centres (Nutman *et al.* 1999; Connelly *et al.* 2000). Thus, the NE-trending suite is dated at 2.04 Ga and will be referred to as the 'Kangâmiut dykes' proper as suggested by Mengel *et al.* (1996).

Although the Kangâmiut dykes have an overall NE trend, there are some systematic deviations. Figure 1 shows that the southern portion of the swarm trends NNE. Moving northward, the orientation gradually changes to ENE. Changes in the orientation of the swarm correlate with increased dyke deformation and recrystallisation. Escher *et al.* (1975) suggested that the bend in the swarm resulted from deformation during the Nagssugtoqidian. Hanmer *et al.* (1997) argue that this change in orientation is a primary feature related to the regional stress field during dyke emplacement.

The majority of dykes south of the Nagssugtoqidian Front retain igneous mineralogies and textures with the exception of a small number of composite dykes with sheared dioritic centres. Shearing was parallel to the dyke contacts, and mostly affected the large composite dykes. Windley (1970) worked in an area just north of Maniitsoq village where he observed cross-cutting dykes. He described a set of cross-cutting dykes where a younger dyke cuts the internal foliation of an older dyke. Not all of the composite dykes show internal deformation. Some dykes show irregular intrusive contacts between the dioritic centre and mafic host dyke showing that they formed by successive injections, closely spaced in time.

Large composite dykes show structural and petrological features not seen in the smaller non-composite dykes. For example, a 140 m wide dyke in Kangerluarsussuaq fjord has fine-grained (*c.* 0.1–0.5 mm) equigranular mafic contacts. Twelve metres from the contact the grain size is *c.* 1 mm with some contact-parallel primary layering. Halfway towards the dyke centre the grain size increases

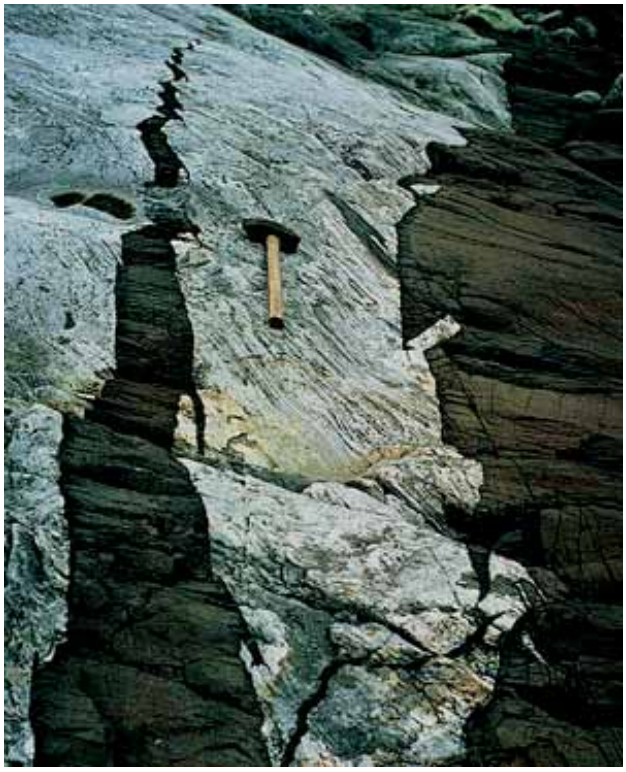

Fig. 2. Kangâmiut dyke with angular bridges within the chilled margin (Photo: David Bridgwater).

to *c*. 3 mm with primary clinopyroxene mostly replaced by hornblende. Near its centre the dyke is slightly foliated and recrystallised to a garnet amphibolite. The centre of the dyke is a strongly foliated garnet-plagioclase-hornblende schist with a dioritic composition. A 10 cm wide epidote-calcite-quartz vein originates from the sheared centre and cuts the non-sheared mafic portion of the dyke.

There are a variety of intrusive relationships between dykes and host rocks including en échelon steps, bridges, and forks. Figure 2 shows bridges with sharp, angular edges contained within the chilled margin of a Kangâmiut dyke. Some dykes have chilled margins up to 40 cm thick, while others have no chilled margins. Chilled margins contain fine-grained plagioclase and clinopyroxene phenocrysts in a microcrystalline groundmass. Some chilled margins contain dismembered bridges of host rock, whereas dyke interiors contain no bridges or xenoliths.

In the northern portion of the dyke swarm, metamorphic minerals and deformation features replace igneous minerals and primary intrusive features. In the Itilleq fjord region, most of the dykes are partly to completely altered during static or shear-related recrystallisation. Some dykes show penetrative foliation, whereas other dykes are deformed only at the contacts and form boudins within the deformed country rock. The central portions of these boudins are partially recrystallised. On the south shore of Itilleq fjord, away from most of the Nagssugtoqidian deformation, the dykes preserve primary emplacement structures, but are statically recrystallised to garnet amphibolites. Dykes at the northern extent of the swarm within Ikertooq fjord are completely recrystallised to granulite facies.

Petrography

The chilled margins of the Kangâmiut dykes contain 0.2–0.8 mm phenocrysts of clinopyroxene and plagioclase in a microcrystalline groundmass of plagioclase, clinopyroxene, hornblende, quartz, and Fe-Ti oxides. Plagioclase phenocrysts are euhedral to subhedral and weakly zoned, whereas the clinopyroxene phenocrysts are subhedral to anhedral. Some chilled margins contain 0.2–1.5 mm hornblende crystals. Figure 3A shows that these hornblende crystals contain abundant inclusions of Fe-Ti oxides, which are absent from the clinopyroxene and plagioclase phenocrysts. These hornblende crystals also enclose plagioclase and clinopyroxene phenocrysts suggesting they are a later phase that crystallised *in situ*.

The interiors of most Kangâmiut dykes are fine- to medium-grained with subophitic textures. Subhedral to anhedral clinopyroxene, plagioclase, and Fe-Ti oxides are the primary constituents along with interstitial quartz, hornblende, and trace amounts of apatite. In some of the dykes, anhedral clinopyroxene fills interstitial areas between subhedral to euhedral plagioclase. Clinopyroxene displays two types of exsolution. The first type is laminar exsolution of low-Ca pyroxene. The second type appears to be granular exsolution of low-Ca pyroxene around the outer parts of the original clinopyroxene crystal. Additionally, most clinopyroxene grains have rims of hornblende (Fig. 3B).

Kangâmiut dyke samples from Itilleq fjord are variably metamorphosed to fine-grained (0.2–1.0 mm) amphibolites with well-developed foliations. Metamorphic assemblages include hornblende, plagioclase, quartz, garnet, titanite, and biotite. Hornblende replaces clinopyroxene, whereas plagioclase and garnet form at contacts between hornblende and plagioclase (see also Mengel *et al.* 1996). Titanite replaces Fe-Ti oxides.

Metamorphic orthopyroxene occurs within Kangâmiut dykes in Ikertooq fjord near the northern extent of the swarm (Fig. 1), marking the transition from amphibolite to granulite facies. The typical assemblage in these granulite facies dykes is plagioclase + hornblende + orthopyroxene + clinopyroxene ± garnet ± titanite (see also Korstgård

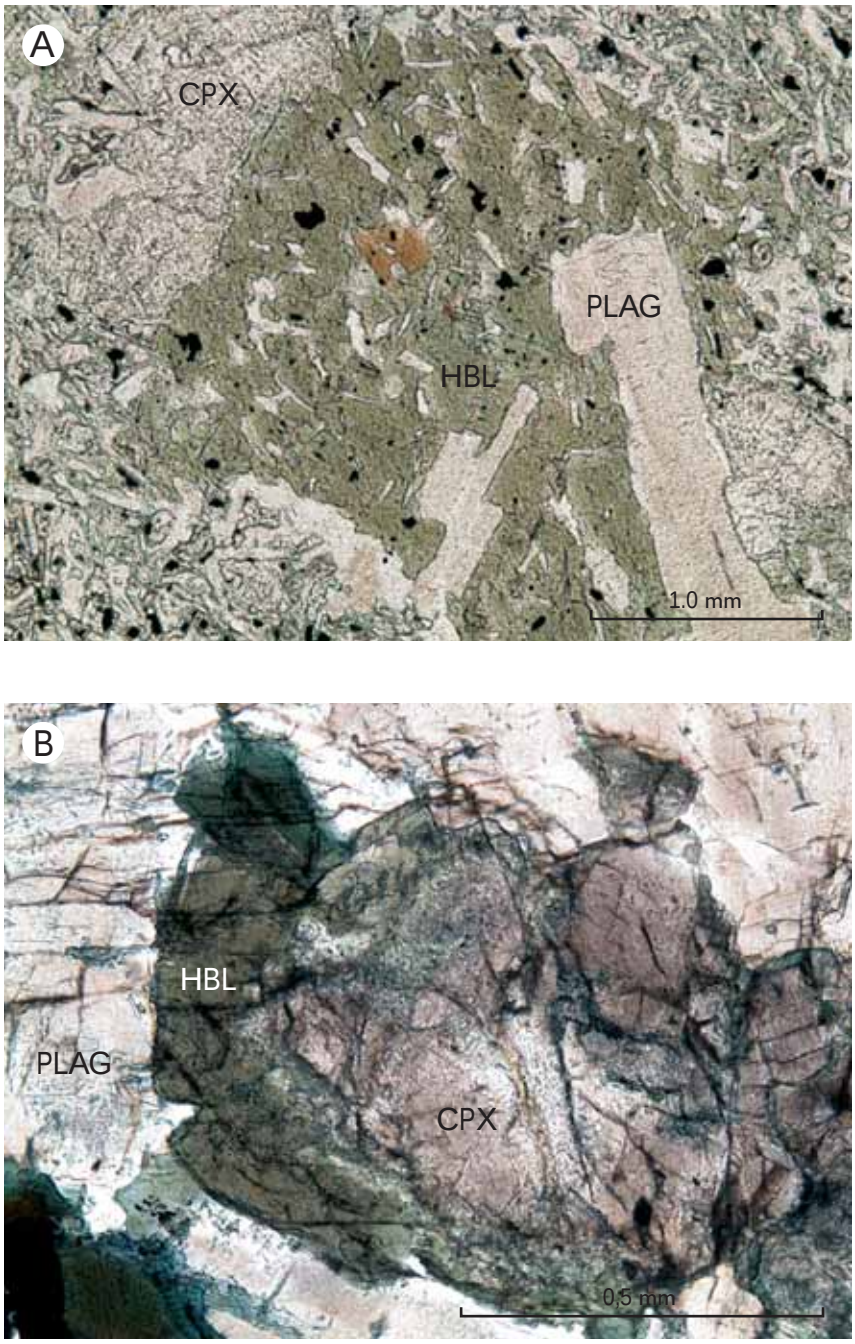

Fig. 3. A: Photomicrograph of a chilled margin of a Kangâmiut dyke with clinopyroxene (CPX) and plagioclase (PLAG) phenocrysts in a groundmass of the same plus Fe-Ti oxides. The large crystal in the centre is hornblende (HBL) with inclusions of a plagioclase phenocryst and groundmass plagioclase and Fe-Ti oxides. Sample GGU 430267, plane polarised light. B: Photomicrograph of a sample from the interior of a Kangâmiut dyke showing hornblende (HBL) rims on clinopyroxene (CPX). Sample GGU 430999, plane polarised light.

1979). These dykes are weakly foliated and fine-grained (0.1–1.0 mm).

Petrology and geochemistry

Whole-rock major and trace elements

A total of 122 dyke samples were analysed for most major and minor elements on fused glass discs using a wavelength dispersive x-ray fluorescence (XRF) spectrometer at the Geological Survey of Denmark and Greenland (GEUS) in Copenhagen. Na_2O was determined by atomic absorption spectrometry. Kystol & Larsen (1999) describe the analytical methods, precision, and accuracy of the GEUS lab and report that the standard error for all major and minor elements is less than 0.25 wt%, based on multiple analyses of international standards.

Trace element concentrations for 73 dyke samples were measured at the University of California-Davis using a

Table 1. Major and trace element data for representative Kangâmiut dykes

Sample	430904	430923	430926	430931	430952	430970	430981	430988	430997	432102	432108	432115	432118	432122	432133	432138	432143	432158
Dyke	5	13	14	16	27	37	42	45	54	86	60	64	64	64	71	70	76	75
SiO_2	50.87	52.78	50.64	50.73	52.19	48.90	50.71	49.30	56.06	57.18	48.97	51.01	56.84	50.25	51.00	49.46	50.57	50.48
TiO_2	2.47	2.31	1.94	0.88	1.62	1.66	1.02	1.45	0.79	1.65	1.69	1.92	2.12	1.82	1.64	2.70	1.33	1.34
Al_2O_3	12.62	13.65	13.29	12.57	13.19	13.14	14.09	13.34	21.46	14.37	13.75	12.97	13.07	13.67	13.96	15.57	13.14	13.59
Fe_2O_3	4.27	3.53	4.26	1.74	4.14	2.52	1.55	1.91	1.24	2.15	4.73	2.21	1.98	2.17	2.06	2.54	1.26	1.75
FeO	11.67	11.34	9.99	9.10	11.05	11.98	9.89	11.40	4.34	8.94	9.48	12.73	10.99	12.22	11.59	11.51	11.99	11.84
MnO	0.24	0.20	0.22	0.21	0.24	0.24	0.21	0.22	0.08	0.16	0.23	0.24	0.19	0.23	0.21	0.20	0.23	0.23
MgO	4.27	3.51	5.55	8.90	4.57	6.40	7.43	6.60	0.92	2.34	6.12	5.08	2.14	5.81	4.78	3.44	6.98	6.12
CaO	8.93	8.24	9.86	12.31	8.48	10.85	11.27	11.39	9.07	6.11	10.72	9.46	6.17	10.12	9.53	8.61	11.40	10.59
Na_2O	2.47	2.91	2.55	2.27	2.80	2.28	2.15	2.25	4.19	3.69	2.44	2.57	3.37	2.45	2.46	2.99	2.11	2.07
K_2O	0.69	1.13	0.58	0.18	0.87	0.28	0.18	0.30	0.51	1.14	0.39	0.52	1.43	0.33	0.47	1.02	0.22	0.35
P_2O_5	0.26	0.29	0.19	0.07	0.19	0.13	0.09	0.13	0.16	0.35	0.15	0.19	0.39	0.10	0.18	0.44	0.10	0.13
LOI	0.84	0.63	0.94	0.91	1.07	1.34	0.79	1.31	0.79	1.43	1.41	1.01	1.17	0.91	1.64	1.35	1.11	1.06
Sum	99.60	100.52	100.03	99.88	100.40	99.72	99.39	99.58	99.61	99.50	100.08	99.90	99.86	100.07	99.53	99.83	100.44	99.55
Sc	38	30	36	58	44	46	47	45	14	20	38	41	22	41	36	29	49	45
V	368	355	333	389	318	381	296	362	29	155	348	393	207	558	303	259	390	336
Cr	47	14	63	145	43	63	153	98	5	33	134	83	22	94	61	33	174	103
Ni	40	28	65	113	40	74	88	60	1	17	82	54	15	66	49	23	78	74
Co	46	44	47	52	44	61	51	56	14	28	53	46	32	54	49	32	53	52
Rb	22	33	16	3.9	25	5.6	4.3	6.1	10	31	7.4	13	45	8.0	12	28	4.6	8.5
Sr	171	201	241	117	207	160	136	160	290	306	235	164	247	164	200	213	138	142
Y	47	34	29	19	35	27	18	27	34	35	26.2	37	48	23	30	53	24	28
Zr	182	168	139	47	133	99	46	92	157	194	106	133	326	78	110	200	58	84
Nb	14.7	10.9	11.8	3.3	9.2	9.2	3.2	8.2	11.3	18.1	9.3	10.0	23.9	6.2	7.3	15.8	4.6	5.2
Ba	204	321	156	50	306	90	50	95	192	392	104	145	454	98	156	366	69	106
La	17.5	20.5	17.1	4.4	12.7	9.2	4.4	8.4	12.3	27.8	10.86	12.9	42.0	7.4	11.4	18.2	5.8	7.6
Ce	43.8	46.0	40.2	10.6	31.9	21.8	10.7	20.7	32.0	63.9	26.28	30.6	94.4	18.1	26.7	40.4	14.1	18.0
Pr	6.07	6.13	5.41	1.49	4.43	3.10	1.70	3.00	4.54	8.66	3.73	4.36	11.96	2.58	3.83	5.58	2.07	2.67
Nd	27.8	27.1	22.7	7.37	18.8	14.2	7.31	13.9	20.6	36.2	16.93	19.1	49.7	11.6	17.3	25.7	9.90	12.2
Sm	7.14	6.11	5.44	2.45	4.58	3.93	2.32	3.71	5.09	8.12	4.35	5.05	10.85	3.02	4.71	6.91	2.72	3.24
Eu	2.08	1.84	1.66	0.82	1.56	1.33	0.89	1.22	1.88	2.49	1.45	1.68	2.93	1.10	1.47	2.20	1.02	1.20
Gd	7.52	6.84	5.55	3.01	5.42	4.51	2.76	4.16	5.41	6.98	4.46	5.27	10.02	3.51	4.86	7.39	3.27	3.99
Tb	1.33	1.12	0.87	0.51	0.95	0.79	0.50	0.73	0.90	1.11	0.75	0.99	1.47	0.60	0.82	1.32	0.57	0.68
Dy	8.17	6.80	5.22	3.12	5.63	4.61	3.10	4.37	5.44	6.31	4.47	6.23	8.26	3.75	5.01	8.56	3.68	4.51
Ho	1.62	1.28	1.06	0.68	1.22	0.99	0.69	0.93	1.15	1.20	0.98	1.24	1.60	0.81	1.08	1.88	0.82	1.04
Er	4.76	3.73	2.96	1.90	3.39	2.75	2.12	2.56	3.23	3.19	2.44	3.71	4.22	2.28	2.92	5.03	2.36	2.89
Tm	0.70	0.52	0.42	0.30	0.52	0.42	0.29	0.38	0.48	0.45	0.34	0.57	0.61	0.34	0.41	0.70	0.36	0.41
Yb	4.52	3.34	2.67	1.97	3.53	2.61	1.96	2.54	3.11	2.89	2.31	3.45	3.90	2.20	2.67	4.97	2.31	2.81
Lu	0.63	0.49	0.39	0.29	0.54	0.42	0.29	0.37	0.45	0.44	0.35	0.55	0.55	0.32	0.43	0.74	0.35	0.41
Hf	4.78	4.60	3.68	1.27	3.54	2.77	1.44	2.47	4.13	4.68	2.83	3.49	7.64	2.10	2.78	5.19	1.59	2.36
Ta	1.03	0.76	0.82	0.26	0.64	0.54	0.24	0.52	0.72	1.27	0.64	0.66	1.55	0.41	0.50	0.98	0.30	0.34
Pb	4.04	5.81	3.26	1.49	6.50	1.84	1.08	3.35	3.78	3.65	1.92	2.63	4.89	1.73	3.07	6.66	1.03	1.88
Th	2.83	3.80	2.12	0.50	3.47	0.90	0.42	0.90	1.88	4.52	1.19	1.73	7.92	1.00	1.61	3.88	0.60	1.04
U	0.71	0.93	0.54	0.14	0.79	0.24	0.11	0.24	0.49	1.10	0.29	0.46	1.92	0.28	0.40	0.87	0.16	0.29

Major element oxides in wt%; trace elements in ppm. Sample numbers refer to GEUS databases. Dyke localities shown in Fig. A1 (appendix).

Perkin-Elmer ELAN 500 inductively coupled plasma mass spectrometer (ICP-MS). Samples were prepared for analyses using the method described by Jenner *et al.* (1990) with the exception that we utilised microwave digestion bombs to insure total dissolution.

Table 1 presents representative major and trace element data for the Kangâmiut dykes, and Figs 4 and 5 show these data in covariation diagrams. The full data set is available upon request from the first author. The Kangâmiut dykes cover a range from 9.0–0.9 wt% MgO and the majority of the dykes would be classified as medium-K basalts or low-K basalts based on their K_2O and SiO_2 contents (Le Maitre 2002). First order observations of the major and compatible trace element data, as described below, indicate that the differentiation of the parental magma(s) of the Kangâmiut dykes was influenced by the fractionation of plagioclase, clinopyroxene, late stage Fe-Ti oxides and possibly olivine. First order observations based on covariation diagrams neither support nor refute the involvement of hornblende as a fractionating phase.

Figure 4C shows Al_2O_3 concentrations that range between 11.4 and 15.8 wt%. The highest MgO sample has a low Al_2O_3 concentration, whereas the next group of dykes at *c.* 7.0–7.5 wt% MgO have higher concentrations of Al_2O_3. This increase of Al_2O_3 between *c.* 9 and 7 wt% MgO likely reflects olivine and/or clinopyroxene fractionation. Clustering of data between 7.5 and 4.5 wt% MgO defines a trend of decreasing Al_2O_3 with decreasing MgO, indicative of plagioclase fractionation. The initial increase in total FeO ($FeO + 0.9 \times Fe_2O_3$) between *c.* 8.0 and 4.5

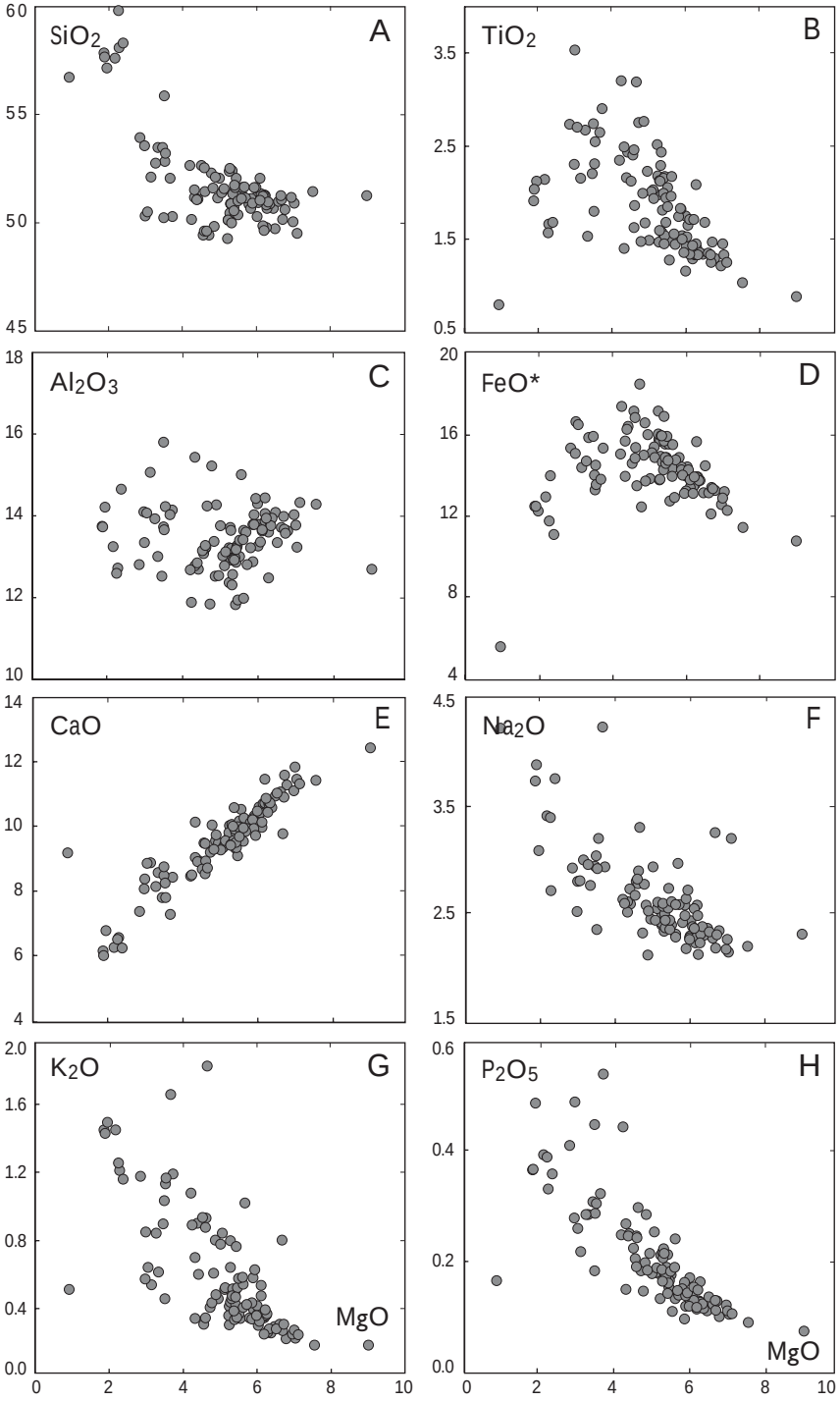

Fig. 4. Variations of SiO_2, TiO_2, Al_2O_3, FeO, CaO, Na_2O, K_2O, P_2O_5 with MgO (in wt%) for the Kangâmiut dykes. All analyses are recalculated on an anhydrous basis with all iron as FeO.

wt% MgO is also indicative of plagioclase fractionation (Fig. 4D).

Figure 4E shows that CaO ranges from 12.4 to 6.0 wt% and correlates positively with MgO, indicating that clinopyroxene and/or plagioclase was part of the fractionating assemblage. Figure 6 shows the CaO/Al_2O_3 ratio for the Kangâmiut dykes decreases with decreasing MgO, and Fig. 5A shows decreasing Sc with increasing Zr. Both of these observations further indicate that clinopyroxene was a fractionating phase. The decrease in nickel with increasing zirconium, shown in Fig. 5C, is related to clinopyroxene and/or olivine fractionation.

Figure 4B shows TiO_2 concentrations that range from 0.9–3.5 wt% with trends that show increasing TiO_2 from 9–4.5 wt% MgO that changes to decreasing TiO_2 below *c.* 4.5 wt% MgO. Figure 4D shows that a similar trend is

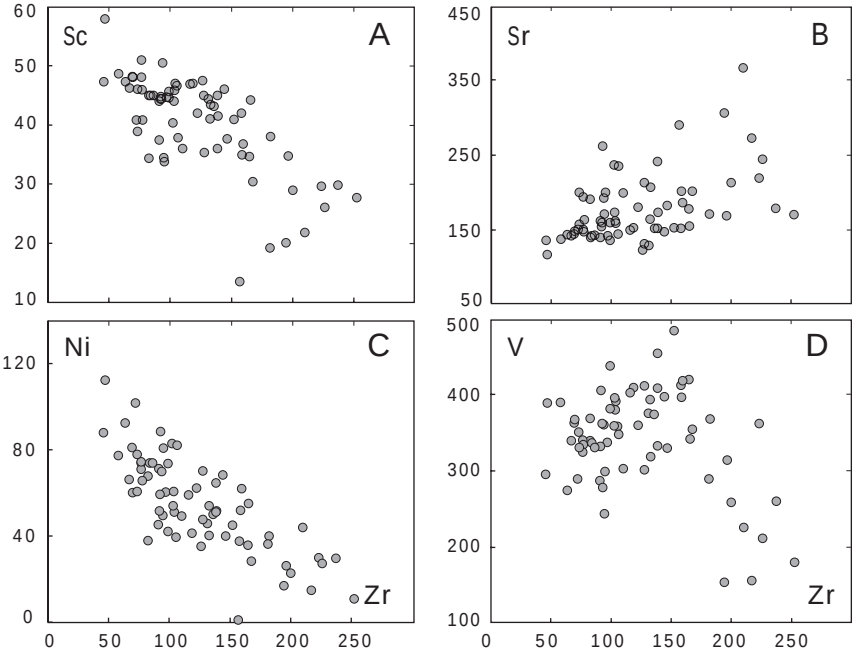

Fig. 5. Variation of Sc, Sr, Ni, and V with Zr (in ppm) for the Kangâmiut dykes.

observed for total FeO. Additionally, vanadium (Fig. 5D) shows an initial increase, then decrease with increasing zirconium. These changes from increasing to decreasing TiO_2, FeO and vanadium concentrations suggest Fe-Ti oxides fractionated when the magmas reached *c.* 4.5 wt% MgO.

Mineral chemistry

Major element compositions of pyroxenes, plagioclase, and hornblende were acquired using a Cameca SX-50 microprobe at the University of California-Davis. Analyses were made using a 15 kV accelerating voltage, a 10 nA beam current, and a 1 µm beam. Elements were calibrated using mineral standards. The data in Tables 2–4 give the compositions of clinopyroxene, plagioclase, and hornblende phenocrysts from chilled margins.

Table 2 presents major and minor element compositions of clinopyroxene phenocrysts from chilled margins based on the average of 2–4 spot analyses of 4–7 grains per sample. The proportions of enstatite, ferrosilite, and wollastonite components are 0.48–0.52, 0.13–0.23, and 0.28–0.35, respectively. Al_2O_3 concentrations range from 3.93–2.75 wt%, while Na_2O varies from 0.36–0.26 wt%.

Table 3 presents plagioclase phenocryst compositions from chilled margins. Plagioclase phenocryst cores have an anorthite (An) component range of An_{69}–An_{55}. Table 4 presents compositions of the hornblendes found in the chilled margins of some Kangâmiut dykes. They would be classified as ferrohornblende and ferrotschermakite based on the classification of Leake *et al.* (1997).

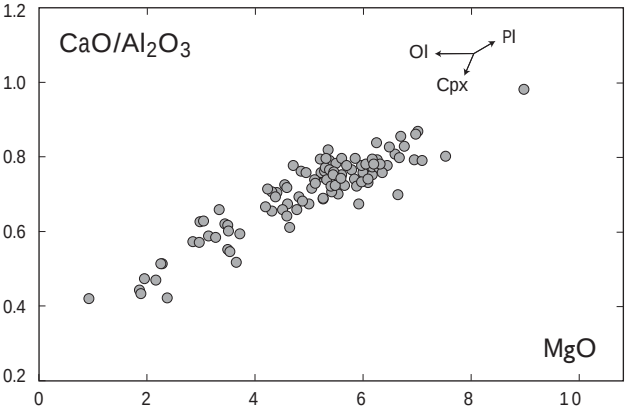

Fig. 6. Variation of CaO/Al_2O_3 with MgO. Arrows show path caused by fractionation of olivine, clinopyroxene, or plagioclase from a starting composition with 9 wt% MgO and Ca/Al_2O_3 = 1.0.

Whole-rock and mineral compositions in projection space

Figure 7 shows pseudo-ternary projections of whole-rock and mineral data for the Kangâmiut dykes. The components CPX, PLAG, OL, and QTZ were calculated using major and minor elements and the scheme of Tormey *et al.* (1987). In the projection from QTZ (Fig. 7A), the dyke data form a cluster that is displaced from the centre

Table 2. Microprobe analyses of clinopyroxene phenocrysts from chilled margins

Sample	430988	432108	432145	432148	432158	430211	430267	430283
Dyke	45	60	76	77	75	82	84	85
	n = 7	n = 8	n = 6	n = 8	n = 8	n = 8	n = 10	n = 10
SiO_2	52.34	50.68	51.88	51.17	52.01	51.36	51.85	51.59
TiO_2	0.47	0.65	0.44	0.61	0.45	0.34	0.44	0.60
Al_2O_3	3.17	3.93	3.14	3.21	3.34	2.75	3.63	2.68
Cr_2O_3	0.11	0.19	0.18	0.21	0.22	0.08	0.18	0.07
FeO	8.29	9.83	8.76	12.45	9.43	13.79	9.72	12.94
MgO	16.46	15.18	15.70	15.62	15.54	16.94	15.62	15.37
CaO	19.59	19.18	18.96	16.16	19.01	14.32	18.01	16.52
Na_2O	0.29	0.32	0.26	0.29	0.28	0.36	0.31	0.26
Sum	100.72	99.96	99.31	99.72	100.28	99.94	99.76	100.03
Si	1.917	1.886	1.927	1.913	1.920	1.922	1.920	1.928
Al(IV)	0.083	0.114	0.073	0.087	0.080	0.078	0.080	0.072
Al(VI)	0.053	0.058	0.065	0.055	0.065	0.074	0.079	0.046
Ti	0.013	0.018	0.012	0.017	0.012	0.011	0.012	0.017
Cr	0.003	0.006	0.005	0.006	0.007	0.001	0.005	0.002
Fe^{3+}*	0.022	0.039	0.000	0.013	0.004	0.016	0.000	0.010
Fe^{2+}	0.232	0.266	0.274	0.377	0.287	0.401	0.308	0.395
Mn	0.000	0.000	0.000	0.000	0.000	0.000	0.000	0.000
Mg	0.899	0.842	0.870	0.871	0.855	0.858	0.862	0.856
Ca	0.768	0.765	0.755	0.647	0.752	0.611	0.715	0.661
Na	0.021	0.025	0.020	0.021	0.020	0.036	0.022	0.019
K	0.000	0.000	0.000	0.000	0.000	0.000	0.000	0.000
Total	4.011	4.020	4.001	4.006	4.002	4.008	3.996	4.005
Mg#	0.78	0.73	0.76	0.69	0.75	0.67	0.74	0.68
Wo	0.35	0.34	0.35	0.29	0.34	0.28	0.33	0.30
En	0.52	0.51	0.50	0.50	0.49	0.49	0.50	0.48
Fs	0.13	0.16	0.16	0.22	0.17	0.23	0.18	0.22

Oxides in wt%; n = number of grains. Fe^{3+}* calculated using the method of Papike *et al.* (1974). Dyke localities shown in Fig. A1 (appendix).

Table 3. Microprobe analyses of plagioclase phenocrysts from chilled margins

Sample	430988	432108	432145	432148	432158	430211
Dyke	45	60	76	77	75	82
	n = 8	n = 8	n = 8	n = 8	n = 7	n = 8
SiO_2	52.18	49.74	53.36	53.79	51.23	54.13
$Al2O_3$	30.45	31.49	29.65	29.65	30.91	29.03
FeO	0.65	0.57	0.59	0.74	0.96	0.92
CaO	13.11	14.13	12.43	12.23	13.34	11.24
Na_2O	4.02	3.36	4.33	4.64	3.89	4.84
K_2O	0.05	0.05	0.09	0.07	0.09	0.17
Sum	100.46	99.34	100.45	101.12	100.41	100.34
Ab	35	30	38	40	34	43
An	64	69	61	59	65	55
Or	0.3	0.3	0.5	0.4	0.5	1.0

Oxides in wt%; n = number of grains. Dyke localities shown in Fig. A1 (appendix).

of the ternary plot towards the PLAG apex. In this projection all the dykes lie within the phase volumes defined by the joins between olivine, clinopyroxene and plagioclase (Ol:Cpx:Pl) or hornblende, clinopyroxene and plagioclase (Hbl:Cpx:Pl). In the projection from the CPX component (Fig. 7B), the dykes define an array that projects away from both the Pl:Ol and the Pl:Hbl joins. Similarly, in the projection from the PLAG component (Fig. 7C), the dykes form an array that intersects both the Cpx:Ol and Cpx:Hbl joins. These observations show that plagioclase, clinopyroxene and either olivine or hornblende were co-fractionating phases.

A and C in Fig. 7 also show experimentally determined 1 atm and 0.8 GPa Ol:Cpx:Pl cotectics derived from melting experiments using a primitive Kangâmiut dyke (dyke #45) as the starting material (Mayborn 2000). The whole-rock data form a cluster near the low pressure Ol:Cpx:Pl cotectic in the projection from the QTZ component. Similarly, in the projection from the PLAG component the whole-rock data also plot close to the low-pressure cotectic.

Incompatible trace element behaviour

Figure 8 shows representative chondrite normalised rare-earth element (REE) patterns for the Kangâmiut dykes. The dykes are slightly light rare-earth element (LREE) enriched with a La/Sm_N ratio ranging from 1.16 to 2.50, with an average of 1.50. The heavy rare-earth (HREE) patterns have shallow slopes with a Dy/Yb_N range of 1.05

Table 4. Microprobe analyses of amphiboles from chilled margins

Sample	432158	430267	430283
Dyke	75	84	85
	n = 12	n = 14	n = 6
SiO_2	43.90	42.63	40.88
TiO_2	1.04	1.92	1.64
Al_2O_3	10.69	10.05	9.98
FeO	21.09	21.73	24.02
MnO	0.22	0.19	0.21
MgO	8.09	8.05	6.44
CaO	10.93	10.78	10.58
Na_2O	1.18	1.63	1.58
K_2O	0.99	0.90	0.90
Cl	0.57	0.67	0.65
F	0.09	0.05	0.14
Sum	98.79	98.60	97.02
Si	6.549	6.425	6.346
Ti	0.117	0.218	0.192
Al(IV)	1.451	1.575	1.654
Al(VI)	0.427	0.209	0.172
Fe^{3+}	0.767	0.799	0.922
Fe^{2+}	1.864	1.940	2.196
Mn	0.027	0.025	0.027
Mg	1.798	1.809	1.491
Ca	1.747	1.741	1.760
Na(M4)	0.253	0.259	0.240
Na(a)	0.089	0.217	0.237
K(a)	0.189	0.172	0.178
Total	15.28	15.39	15.41

Oxides, Cl and F in wt%. Dyke localities shown in Fig. A1 (appendix).

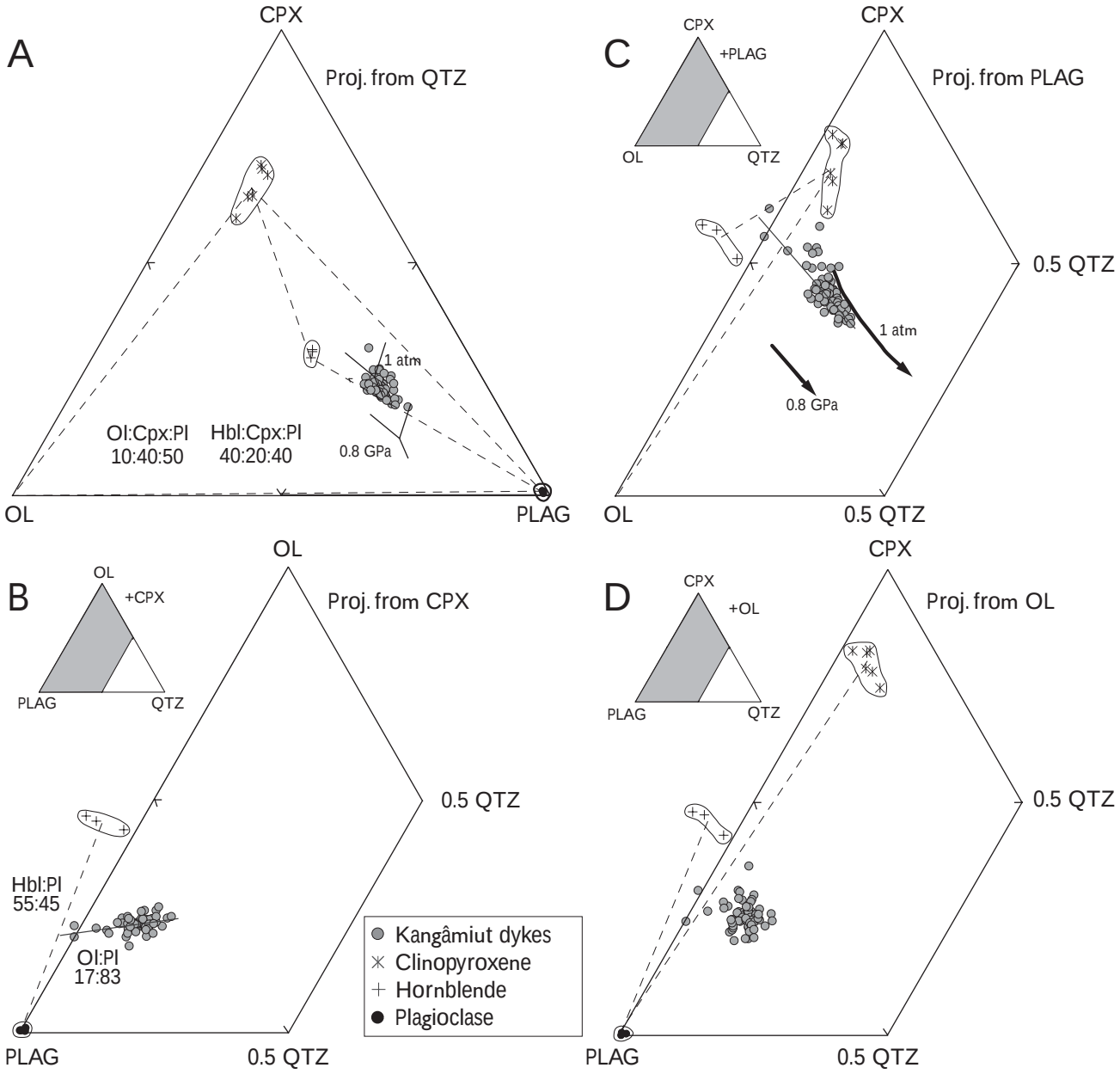

Fig. 7. Pseudo-ternary projections of whole-rock and mineral compositions from the Kangâmiut dykes using the projection scheme of Tormey *et al*. (1987). Dashed lines connect possible crystallisation assemblages. Solid lines through data show the trend of Kangâmiut dykes where this is well defined, and the locations of the olivine:clinopyroxene:plagioclase cotectics at 0.8 GPa and 1 atm. A: Projection from the QTZ component. B: Projection from the CPX component. C: Projection from the PLAG component. D: Projection from the OL component.

to 1.46 and an average of 1.15. The two most LREE-enriched samples come from sheared dioritic centres and have Dy/Yb_N ratios of 1.46 and 1.42, respectively. The patterns for the sheared dioritic centres cross-cut the patterns for non-sheared dykes.

Figure 9A shows incompatible trace elements for the Kangâmiut dykes on primitive mantle normalised compatibility diagrams (Thompson 1982). The elements on the right hand side of Fig. 9A are moderately incompatible, with incompatibility increasing towards the left using the element order from Sun & McDonough (1989). The most primitive Kangâmiut dykes have the lowest concentration of incompatible elements and have flat patterns with small negative Nb and Zr anomalies. The negative Sr anomaly seen in the more evolved samples reflects plagioclase fractionation. The two most evolved samples

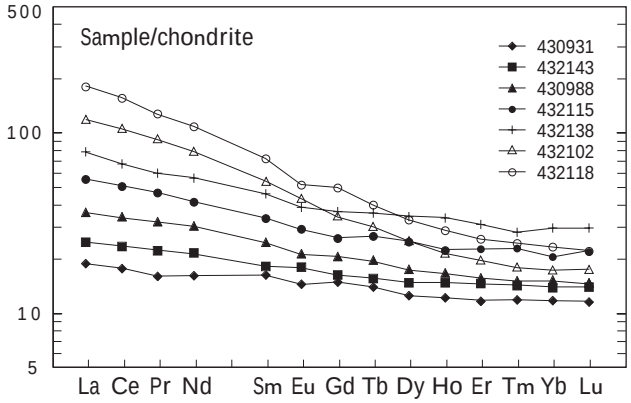

Fig. 8. Rare-earth element compositions of representative Kangâmiut dykes normalised to C1 chondrite. Chondrite normalising values from Sun & McDonough (1989).

(432102 and 432118) are sheared dioritic centres and display negative Ti anomalies. They also show a depletion of HREE, as noted in Fig. 8.

Figure 9B shows representative patterns for basalts from a variety of tectonic settings and a pattern representing the average of Kangâmiut dykes with MgO > 6 wt%. Notable features in the Kangâmiut pattern are a smooth, slightly increasing trend from right to left through the moderately incompatible elements (Lu to Sm), small negative anomalies of Nb, Sr, and Zr, and a relatively flat trend for Th, Ba and Rb. The Kangâmiut dyke pattern is distinct relative to the ocean island basalt (OIB), mid-ocean ridge basalt (MORB), island arc basalt (IAB), and continental arc basalt (CAB) patterns. For example, the Kangâmiut dykes do not display the enrichment of highly incompatible elements, or the positive Nb anomaly seen in the OIB pattern, or depletions seen in the MORB pattern. Relative to IAB and CAB, the Kangâmiut dyke patterns do not exhibit the large negative Nb anomaly or the positive Sr anomaly. Overall, the Kangâmiut dyke pattern most closely resembles the pattern for continental flood basalts (CFB), including the shallow slope of the pattern, and the small negative Nb and Sr anomalies.

Discussion

Tectonic setting

One of the primary goals of this study is to constrain the tectonic environment during emplacement of the Kangâmiut dykes. Experimental melting studies over the past 40 years have shown that basalts are products of partial melting of peridotite (Reay & Harris 1964; Takahashi 1986; Baker & Stolper 1994). Since the dominant source of peridotite is the mantle, then the basaltic nature of the Kangâmiut dykes indicates that they resulted from partial melting of mantle peridotite followed by intracrustal differentiation. Three settings where mantle melting occurs beneath continental crust are (1) subduction zones, (2) active rifts associated with mantle plumes, and (3) passive rift settings. Each of these settings can have distinctive mantle compositions and conditions for melting

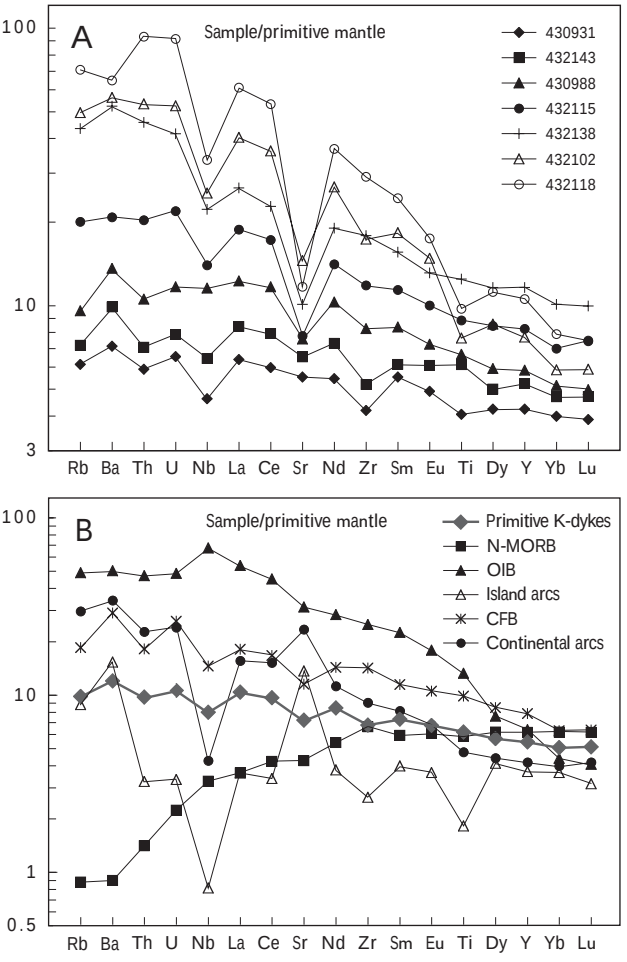

Fig. 9. A: Normalised incompatible trace element compositions of representative Kangâmiut dykes. B: Comparison of the Kangâmiut dykes with normal mid-ocean ridge basalts (N-MORB), ocean-island basalts (OIB), island arc basalts, continental flood basalts (CFB), and continental arcs. Representative 'Primitive Kangâmiut dykes' is the average composition of 18 Kangâmiut dykes with a MgO range of 8.9–6.1 wt%. Data for N-MORB and OIB are from Sun & McDonough (1989). Island arc data compiled from Bailey *et al.* (1989), Pearce *et al.* (1995), and Gust *et al.* (1997). CFB data compiled from Hooper & Hawkesworth (1993), Lightfoot *et al.* (1993), Wooden *et al.* (1993), Peate & Hawkesworth (1996) and Storey *et al.* (1997). Continental arc data compiled from Tormey *et al.* (1991) and Bacon *et al.* (1997).

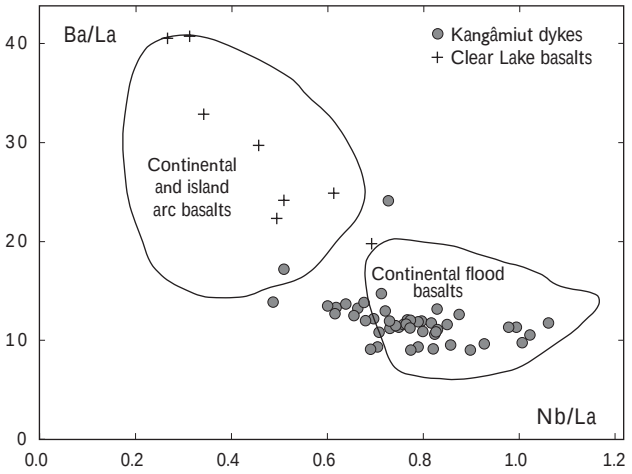

Fig. 10. Ba/La versus Nb/La showing the differences between arc basalts, the Kangâmiut dykes, and basalts from the Clear Lake Volcanic Field. Data for the arc field are from Bailey *et al.* (1989), Tormey *et al.* (1991), Francalanci *et al.* (1993), Pearce *et al.* (1995), Bacon *et al.* 1997), Gust *et al.* (1997), and Kelemen *et al.* (2003). Data for the continental flood basalt field are from Hooper & Hawkesworth (1993), Lightfoot *et al.* (1993), Wooden *et al.* (1993), Peate & Hawkesworth (1996), and Storey *et al.* (1997). Data for the Clear Lake Volcanic Field are from Charles Lesher (unpublished data).

that are reflected in the trace element compositions of the associated basalts.

The Kangâmiut dykes have evolved compositions with a Mg-number (defined as 100Mg/(Mg + Fe) on a molecular basis) range of 0.60–0.21. Magmas in equilibrium with mantle peridotite will have a Mg-number close to 0.71 (Roeder & Emslie 1970; Langmuir *et al.* 1992) showing that even the most primitive Kangâmiut dykes represent somewhat evolved magmas. Thus, the major elements reflect both the fractionation and mantle melting histories. However, most incompatible trace element ratios remain relatively constant during crystallisation and can be used to constrain primary source characteristics. The following discussion examines some characteristics of the mantle source and the conditions of mantle melting revealed by examining incompatible trace elements from the more primitive dyke samples (with MgO > 4.5 wt%).

Subduction hypothesis for generation of Kangâmiut dykes

Subduction environments generate basaltic melts by two different mechanisms of partial melting. The first is melting induced by lowering the solidus temperature of the peridotite by the introduction of volatiles from the subducting slab and subsequent decompression melting within the mantle wedge (Jakes & Gill 1970; Tatsumi 1989; Arculus 1994). The second is decompression melting associated with back-arc spreading (Tatsumi *et al.* 1989; Gribble *et al.* 1998). Although the mechanisms of melting in these settings are different from each other, they both produce magmas with a compositional 'subduction component' that is indicative of a hydrated and metasomatised mantle. Some important characteristics of subduction zone basalts are HFSE depletions, LILE enrichment, and high Al_2O_3. The available data can be used to evaluate the subduction hypothesis for the Kangâmiut dyke swarm implied by Escher *et al.* (1976) and Bridgwater *et al.* (1995), and explicitly proposed by Cadman *et al.* (2001).

As shown in Fig. 9B, arc basalts have distinctive depletions in HFSE. These HFSE depletions occur in Palaeozoic, Proterozoic, and Archaean arc-related basalts, suggesting that modern style subduction occurred in the Archaean (Stern *et al.* 1994; Blichert-Toft *et al.* 1995). In addition to HFSE depletions, arc basalts are enriched in LILE (e.g. Pb, K, Ba, Rb, and Cs) relative to basalts from other tectonic settings. This enrichment is proposed to

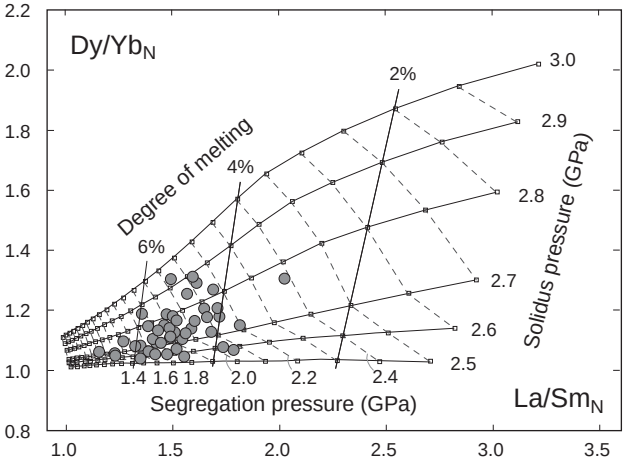

Fig. 11. Chondrite-normalised DyYb versus La/Sm ratios for the Kangâmiut dykes and mantle melting models using the algorithm of Fram & Lesher (1993) based on a 0.5% depleted PM source composition, where F is the melt proportion. The model assumes partial melting proceeds by incremental non-modal batch melting at 1% per kbar of decompression in a corner flow melting regime. Melts are pooled after each kbar of decompression. REE distribution coefficients are taken from Green (1994). The garnet-spinel transition is modelled as a gradual change between 30 and 25 kbar. The spinel–plagioclase transition is modelled as a gradual change between 14 and 10 kbar. Residues are recalculated after each melting increment and adjusted for pressure dependent phase transitions using melting reactions as given by Fram & Lesher (1993). Model curves, for melting starting at 3.0, 2.9, 2.8, 2.7, 2.6 and 2.5 GPa and ending at 0.5 GPa, define a melting grid, where solid subvertical lines contour constant mean melt fraction, whereas the dashed subvertical lines contour final pooled melt segregation pressure (i.e. the top of the melting column). Slightly modified from Mayborn & Lesher (2004).

occurduring the flux of fluids from the slab into the mantle wedge (Miller *et al.* 1994; Pearce *et al.* 1995; Becker *et al.* 1999). Mafic rock suites in volcanic arc settings also typically contain a large proportion of high-alumina basalts (Perfit *et al.* 1980; Brophy & Marsh 1986; Kelemen *et al.* 2003).

If the Kangâmiut dykes are arc-related, they should show LILE enrichment, HFSE depletions, and high Al_2O_3. Figure 10 shows a comparison of the Nb/La and Ba/La ratios for the Kangâmiut dykes, island arcs, continental arcs, and continental flood basalts. Relative to arc basalts, the Kangâmiut dykes have lower Ba/La and Nb/La ratios – unlike arc-related basalts. Additionally, subduction zone basalts typically have Al_2O_3 contents of 19–15 wt% (Plank & Langmuir 1988, 1992; Kelemen *et al.* 2003), whereas all of the Kangâmiut dykes have lower Al_2O_3 concentrations (16–12 wt%). Thus, the Kangâmiut dykes have none of the geochemical characteristics of subduction related basalts, contrary to previous conjecture (Cadman *et al.* 2001).

A more detailed analysis of the Cadman *et al.* (2001) hypothesis also raises significant questions about its viability. Cadman *et al.* (2001) propose that the Kangâmiut dykes formed after ridge subduction resulting in a 'slab window' passing beneath metasomatised mantle. The resulting mantle upwelling lead to melting within hydrated mantle wedge material. Although Cadman *et al.*'s hypothesis would explain elevated water contents postulated for Kangâmiut dyke magmas, such an origin would also be expected to impart an arc geochemical signature to the magmas. It is instructive to directly compare the composition of the Kangâmiut dykes with those from the Clear Lake Volcanic Field located in the coastal region of northern California and associated with the development of a slab window after passage of the Mendocino Triple Junction (Furlong & Schwartz 2004). Figure 10 compares the Ba/La and Nb/La ratios for Clear Lake basalts, with typical arc basalts, the Kangâmiut dykes and continental flood basalts. It is evident from these, among other, geochemical indices that the Kangâmiut dykes lack the expected arc signature postulated by Cadman *et al.* (2001). Rather the Kangâmiut dykes have compositions consistent with their derivation from asthenospheric mantle supplying normal continental flood basalts.

Active rifting, plume and passive rifting hypotheses

The temperature of the mantle is an important difference between plume associated rifting and passive rifting. Mayborn & Lesher (2004) presented a detailed analysis of the

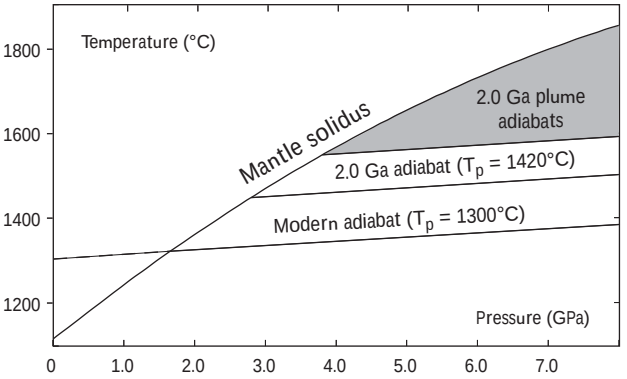

Fig. 12. Plot showing the fertile peridotite solidus and adiabats for modern mantle, 2.0 Ga mantle, and plume mantle associated with potential temperatures of 100 to 300°C greater than 2.0 Ga mantle. Pressures and temperatures for the fertile peridotite from Hirschmann (2000). Slightly modified from Mayborn & Lesher (2004).

temperature of the mantle during Kangâmiut dyke magma genesis as constrained by REE systematics. They used the algorithm of Fram & Lesher (1993), as shown in Fig. 11, to propose that the Kangâmiut dykes are the results of mantle melting with a mean solidus pressure of *c.* 2.75 GPa and a mean extent of melting of 5%. When compared to the solidus for nominally anhydrous mantle (Fig. 12), this mean solidus temperature would correspond with a potential mantle temperature of 1420°C. This temperature estimate falls at the lower end of potential temperatures estimated for *c.* 2.0 Ga mantle by Richter (1984, 1420–1600°C) and Abbott *et al.* (1994, 1380–1680°C) based on secular cooling models and geochemical data for Precambrian MORB-type basalts, respectively. Addition-

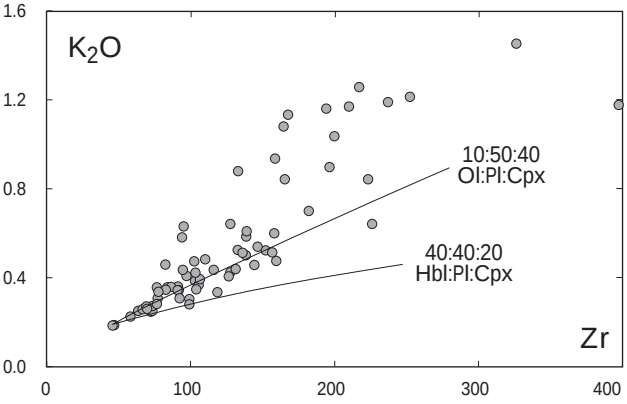

Fig. 13. Variation of K_2O (in wt%) with Zr (in ppm) for the Kangâmiut dykes. Solid lines show results of fractional crystallisation models using mineral proportions of 10:50:40 Ol:Pl:Cpx and 40:40:20 Hbl:Pl:Cpx. The model starting composition is the sample with lowest K_2O and Zr, which are 0.19 wt% K_2O and 47 ppm Zr. Based on Cadman *et al.* (2001).

ally, an ambient mantle potential temperature of 1420°C at 2.0 Ga. is consistent with constraints from continental freeboard that suggests that mantle temperatures were below 1430°C by the mid-Archaean (Galer 1991). Thus, the 1420°C mantle temperature for the Kangâmiut dykes is consistent with ambient mantle temperatures for that time, reducing the need for anomalously high potential temperatures commonly associated with plume magmatism. The explanation that best fits both the geochemical and field data is that the Kangâmiut dykes formed by decompression melting in a rift environment under ambient mantle conditions. This conclusion implies that the dykes are the products of rifting of Kenorland supercontinent between 2.1 and 2.0 Ga (Williams *et al.* 1991). The implications of these findings for the temperature of the Palaeoproterozoic mantle, the occurrence of Palaeoproterozoic mantle plumes, and for Palaeoproterozoic continental crustal growth are discussed in Mayborn & Lesher (2004).

Fractionation of the Kangâmiut dykes

As noted previously, the range in Mg-number (0.60–0.21) of the Kangâmiut dykes shows that they are not in equilibrium with mantle peridotite and do not represent direct mantle melts. Thus, even the most primitive sampled Kangâmiut dyke represents an evolved magma. First order observations of the whole-rock and mineral data show that the dykes evolved by Ol:Cpx:Pl or Hbl:Cpx:Pl fractionation with the late-stage introduction of Fe-Ti oxides into the fractionating assemblage. Windley (1970) and Bridgwater *et al.* (1995) proposed that hornblende was a primary crystallising phase from the Kangâmiut dyke magmas partly based on the occurrence of large hornblende crystals in chilled margins. However, our petrographical studies of the chilled margins show that these amphiboles grew *in situ* during the final stage of solidification (see Fig. 3). This does not preclude the possibility that hornblende was a stable and fractionating phase at depth and thus influenced the composition of evolved Kangâmiut dyke magmas prior to their emplacement.

The main difference between Hbl:Cpx:Pl and Ol:Cpx:Pl crystallisation to explain the magmatic evolution of the dykes is the relative cotectic proportions of hornblende and olivine. In the projection from QTZ (Fig. 6A) the dyke compositions lie within both the Hbl:Cpx:Pl and Ol:Cpx:Pl phase volumes. If hornblende is a fractionating phase its cotectic proportion would be *c.* 0.40 (based on the projections from QTZ, CPX, and PLAG), with plagioclase and clinopyroxene at 0.40 and 0.20, respectively. If olivine, and not hornblende, is a fractionating phase, the cotectic proportions would be *c.* 0.10 olivine, 0.50 plagioclase, and 0.40 clinopyroxene.

These different cotectic proportions can be used to determine if hornblende or olivine was a fractionating phase by examining the partitioning behaviour of potassium. Experimentally determined amphibole-basaltic melt Kds for potassium range between 1 and 2 (Green 1994). In contrast, the olivine-basaltic melt Kd is *c.* 0.0005 (Green 1994) for potassium between olivine and basaltic liquid. Figure 13 shows the results of fractional crystallisation modelling for K_2O and Zr. The cotectic assemblage 40:40:20 Hbl:Cpx:Pl gives a bulk distribution coefficient (D) of 0.52 for K and 0.094 for Zr. The olivine-bearing assemblage, 10:50:40 Ol:Cpx:Pl, gives a bulk D of 0.16 for K and 0.026 for Zr. As shown in Fig. 13, the hornblende-bearing assemblage underestimates the concentration of K_2O and is not consistent with the trend defined by the dyke data, whereas the olivine-bearing assemblage provides a better fit to the data. Thus, these relationships show that the Kangâmiut dykes evolved by the fractionation of olivine, clinopyroxene, plagioclase and late stage Fe-Ti oxides, and that hornblende was not a significant fractionating phase at any stage of their evolution. Support for this conclusion comes from the 0.8 GPa melting experiments of Mayborn (2000) showing that the cotectic assemblage for a water-bearing Kangâmiut dyke starting material is olivine, clinopyroxene, and plagioclase, but no hornblende.

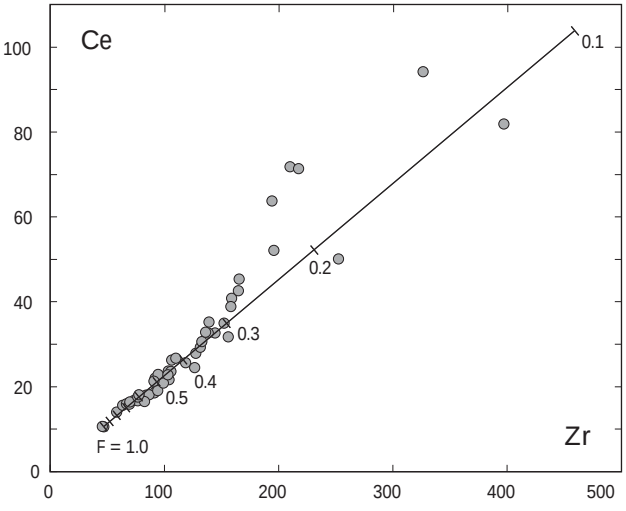

Fig. 14. Variation of Ce with Zr (in ppm) showing the results of a fractional crystallisation model where F is the melt proportion. Tic marks on model curve are drawn at 0.1 intervals of F.

Origin of water in the Kangâmiut dykes

Based on the presence of hornblende in the Kangâmiut dykes, Bridgwater *et al.* (1995) speculated that the parental magmas for the dykes were derived from a hydrous protolith during thrusting of an amphibolite facies terrain beneath the granulite facies terrain in the southern Nagssugtoqidian orogen. Although this model does offer an explanation for the proposed high water contents of the dykes, the presence of hornblende itself, often as reaction rims on clinopyroxene or poikilitic grains enclosing plagioclase and clinopyroxene, only argues for elevated water contents during final stages of crystallisation of the dykes. It is, therefore, possible that the high water contents sufficient to stabilise hornblende resulted solely from its enrichment during crystal fractionation.

The modal abundance of hornblende in dykes not affected by Nagssugtoqidian deformation is *c*. 5–20% for dolerites and 10–35% for dioritic centres. Since amphiboles contain *c*. 2 wt% water, these modes would indicate a whole-rock water concentration of 0.1 wt% in the primitive dolerites and 0.7 wt% in the more evolved dioritic centres. Whether these differences in concentrations between the primitive and evolved samples are related to enrichment during crystal-liquid fractionation can be evaluated using the following equation for fractional crystallisation:

$$C_L = C_0 \times F^{(D-1)} \qquad (1)$$

where C_0 is the initial concentration, C_L is the liquid concentration, F is the proportion of liquid, and D is the bulk distribution coefficient. Danyuschevsky *et al.* (2000) showed that in mafic systems water will have a bulk distribution coefficient of *c*. 0.01. Starting with a magma with 0.1 wt% (C_0) H_2O, representing the primitive dolerites, and ending with 0.7 wt% (C_L) H_2O, representing the evolved dioritic centres, requires 86% crystallisation (F = 0.14) of the primitive magma. Figure 14 shows the relative enrichment of highly incompatible elements Zr and Ce during fractional crystallisation, where Ce is used as a proxy for water given their similar incompatibilities (Danyuschevsky *et al.* 2000). The amount of fractionation required to relate the primitive samples to dioritic centres is 0.3–0.13, corresponding to 70–87% crystallisation. Thus, the evolved dykes reflect sufficient fractionation to explain the difference in water concentrations between the primitive dykes and dioritic centres.

The origin of the water in the primitive dykes can also be addressed using equation 1. The most primitive Kangâmiut dykes (MgO > 6 wt%) have a modal hornblende content of 5–10% indicating a maximum of 0.1–0.2 wt% water content in the rocks. This suggests that the amount of water in the parental magma derived from the mantle is less than 0.2 wt%. Equation 1 can also approximate fractional mantle melting and can help constrain the amount of water in the mantle source needed to produce a primitive magma containing 0.2 wt% H_2O. In this case, the unknown variable is C_0, the initial concentration in the mantle. The concentration in the liquid (C_L) is 0.2 wt%, and D is equal to 0.01. The evaluation of REE systematics, presented by Mayborn & Lesher (2004) and illustrated in Fig. 11, shows that the average F value for mantle melting leading to the Kangâmiut dykes was 0.05. Thus, using these values in equation 1 results in a concentration in the mantle source (C_0) of 0.01 wt% (100 ppm). This is well within the range of 28–300 ppm H_2O given by Bell & Rossman (1992) for the upper mantle containing nominally anhydrous phases. As such, the water present in the hornblende within the Kangâmiut dykes can be reasonably accounted for given estimates of its original concentration in primary melts and enrichment through subsequent differentiation. Although these considerations do not rule out Bridgwater *et al.*'s (1995) model for the Kangâmiut dykes derived from an amphibolite facies protolith, we show that differentiation of partial melts derived from depleted upper mantle can readily explain the occurrence of late crystallising hornblende in the evolved Kangâmiut magmas.

The Kangâmiut dykes and the Nagssugtoqidian orogeny

The preservation of both igneous and metamorphic features in the Kangâmiut dyke swarm provides an excellent opportunity to evaluate the amount of crustal thickening that likely occurred during the Nagssugtoqidian orogeny. Determining the amount of thickening requires knowledge of the depths associated with emplacement and peak metamorphism for currently exposed dykes.

Field relationships show brittle deformation of host rocks and segmentation of the Kangâmiut dykes into en échelon arrays during emplacement. Reches & Fink (1988) proposed that the segmentation of dykes into en échelon arrays occurs when they cross from the ductile into the brittle regime. In modern continental crust the brittle–ductile transition is observed as the seismic to aseismic transition at depths of 10–15 km (Chen & Molnar 1983). Chen & Molnar (1983) and Williams (1996) give temperature estimates for the brittle–ductile transition between 450 and 250°C.

Fahrig & Bridgwater (1976) presented Palaeomagnetic data from dykes and host rocks unaffected by Nagssugtoqidian metamorphism, and showed that the host rocks and dykes record different declinations. These differences in declination show that the host rocks were below their Curie temperature during dyke emplacement. Fahrig & Bridgwater (1976) do not discuss the magnetic carrier in the host rocks, but an examination of host rock samples suggests that the magnetic carrier(s) are magnetite and/or ilmenite. The Curie temperatures of these minerals vary due to solid solutions amongst magnetite-ulvöspinel and hematite-ilmenite, but the upper limit is 580°C if the magnetic carrier is pure magnetite.

Additional support for dyke emplacement into host rocks with temperatures below 580°C comes from $^{40}Ar/^{39}Ar$ dating of dykes and host rocks. Willigers *et al.* (1999) presented $^{40}Ar/^{39}Ar$ cooling ages from dykes in the southern foreland that gave a mean age of 2.02 Ga. This age is within error of the 2.04 Ga emplacement age determined by dating of igneous zircons (Nutman *et al.* 1999). The $^{40}Ar/^{39}Ar$ cooling age of a regional granitic host rock is 2.5 Ga (Willigers *et al.* 1999). This older age indicates that the host rocks have remained below 480°C, the closure temperature of argon in hornblende (Harrison 1981), since 2.5 Ga.

Field evidence of brittle deformation, Palaeomagnetic data, and $^{40}Ar/^{39}Ar$ cooling ages all indicates that the peak crustal temperatures of exposed basement hosting the Kangâmiut dykes were less than *c*. 450°C at the time of dyke emplacement. Estimates of the geothermal gradient appropriate for continental crust at 2.0 Ga can help to constrain the depth of the 450°C isotherm and thus the depth of dyke emplacement. The geotherm is computed from

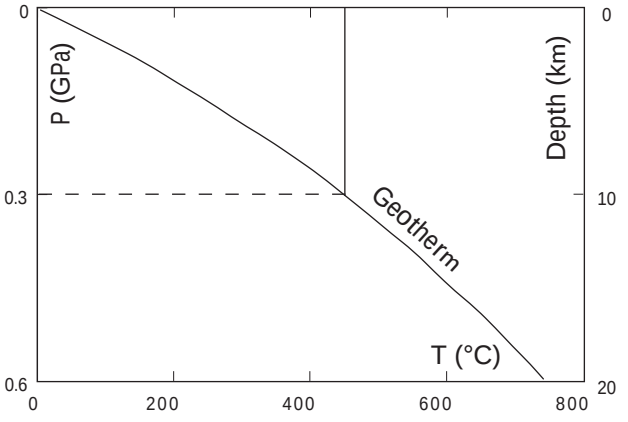

Fig. 15. Model continental geotherm constructed using the heat flow equation shown in text (equation 2). Solid vertical line represents the 450°C isotherm that intersects the geotherm at *c*. 0.3 GPa (10 km) as shown by dashed horizontal line.

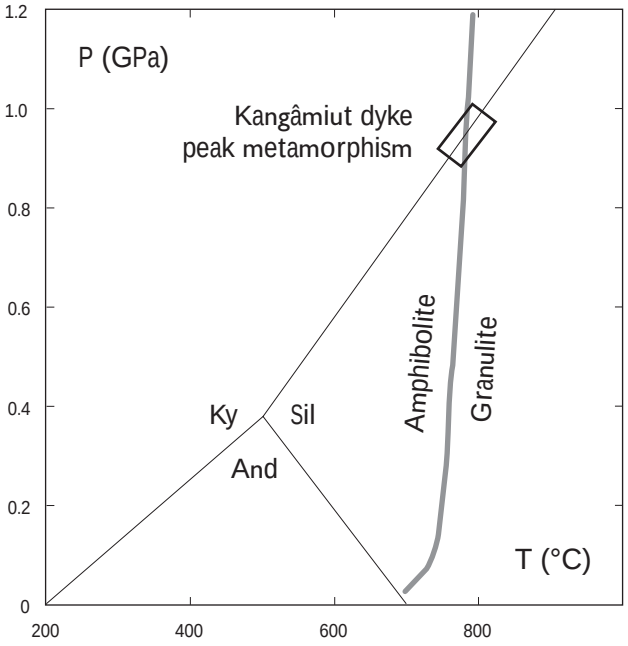

Fig. 16. Pressure versus temperature diagram showing the intersection of the amphibolite/granulite facies transition with the kyanite–sillimanite transition. The black rectangle around the intersection shows possible temperature and pressure ranges of peak metamorphism of the Kangâmiut dykes and metasediments in Ikertooq fjord. The Al_2SiO_5 phase diagram is from Holdaway (1971) and the amphibolite to granulite transition is based on the first occurrence of orthopyroxene in experiments on mafic rocks by Spear (1981).

the heat flow equation assuming an exponential distribution of heat producing elements that includes contributions from heat conduction, advection, and production (Carslaw & Jaeger 1959):

$$T = \frac{Q^* z}{k} + \frac{A^o D^2}{k}\left(1 - e^{-z/Hr}\right) \qquad (2)$$

where T is temperature in °C, Q* is the reduced heat flow at the crust-mantle boundary in mWm^{-2}, z is the depth in km, k is the thermal conductivity of the crust in $Wm^{-1}K^{-1}$, A^o is the concentration of heat producing elements at the earth's surface in μWm^{-3}, D is crustal thickness in km, and Hr is the length scale for the decrease in heat producing elements with depth in km. Current average values are Q = 30 mWm^{-2}, k = 2.25 $Wm^{-1}K^{-1}$, A^o = 0.75 μWm^{-3}, D = 35 km, and Hr = 15 km. The model geotherm shown in Fig. 15 uses these values with the exception of A^o = 1.2 to account for higher heat production during the Palaeoproterozoic and Archaean (Stein 1995). Using the geotherm in Fig. 15 and a maximum host rock tempera-

ture of 450°C require that the dykes intruded to a minimum depth of 10 km corresponding to a lithostatic pressure of *c*. 0.3 GPa. This estimate of a shallow emplacement level for the dykes is also supported by the clustering of whole-rock data near the low-pressure Ol:Cpx:Pl cotectics as previously shown in Fig. 7.

Application of the clinopyroxene geothermobarometry developed by Putirka *et al.* (1996) provides another independent estimate of the depth of dyke emplacement. This geothermobarometer uses compositions of clinopyroxenes and their host rocks to estimate the pressure and temperature of clinopyroxene crystallisation. There are two important assumptions when applying this geothermobarometer to chilled margins in the Kangâmiut dykes. First, we assume that the whole-rock composition is a close approximation of the original liquid composition. Second, we assume that the cores of the clinopyroxene phenocrysts were once in equilibrium with this liquid. One test of equilibrium between the whole-rock and clinopyroxene phenocrysts is given by the FeO/MgO ratios in the whole rocks and pyroxenes. The FeO/MgO ratios in the clinopyroxenes from eight chilled margins and the FeO/MgO ratio in their host rocks yield an average $K_D^{Fe\text{-}Mg}$ for clinopyroxene and liquid of 0.32 ± 4. Based on experimental work, $K_D^{Fe\text{-}Mg}$ for basaltic systems between 1 atm and 1.5 GPa ranges from 0.22–0.36 (Baker & Eggler 1987; Putirka *et al*. 1996). Our estimates for the Kangâmiut dykes fall within this range.

Applying the Putirka *et al.* (1996) geothermobarometer to clinopyroxene phenocrysts cores and whole-rock compositions from chilled margins of eight Kangâmiut dykes gives temperatures of 1199–1170°C and pressures of 0.75–0.35 GPa. The upper pressure limit of 0.75 GPa indicates a maximum recorded depth of fractionation recorded by clinopyroxene phenocrysts of *c*. 25 km. The lower pressure estimate of 0.35 GPa constrains a maximum emplacement depth of *c*. 12 km, since the clinopyroxene phenocrysts in the chilled margins must have formed at a depth greater or equal to the final depth of dyke emplacement. This is consistent with the preceding results from temperature estimates of the host rocks during emplacement that indicate a maximum of *c*. 0.3 GPa or a depth of *c*. 10 km.

If these independent estimates of the Kangâmiut dyke emplacement depths are taken as representative of the dyke swarm in general, then a consideration of peak metamorphic conditions during the Nagssugtoqidian orogeny can be used to constrain the amount of crustal thickening during orogenesis. The majority of the metamorphism of the northern portion of the swarm during the Nagssugtoqidian orogeny occurred at amphibolite facies, with the exception of the northernmost portion within Ikertooq fjord where the transition to granulite facies metamorphism occurs. The amphibolite to granulite facies transition is marked by the first appearance of orthopyroxene in mafic rocks and is known to occur at *c*. 800°C (Spear 1981). The constraint on the pressure of the granulite facies metamorphism comes from the presence of kyanite-sillimanite paragneisses that are interleaved with sheets of dyke-bearing orthogneisses. The presence of granulite facies metamorphosed Kangâmiut dykes and the alumina-silicate-bearing gneisses indicates that peak metamorphism occurred at conditions corresponding to both the amphibolite to granulite and kyanite to sillimanite transitions. Figure 16 shows that these transitions indicate a peak metamorphic pressure of *c*. 0.9 GPa. This pressure is consistent with the results of Mengel *et al*. (1995) who determined metamorphic pressures on the Kangâmiut dykes in the Ikertooq region using TWEEQU geothermobarometry (Berman 1991).

Knowing the approximate depth of emplacement and the pressure of peak metamorphism provides constraints on the amount and style of burial during the Nagssugtoqidian orogeny. Emplacement at 0.3 GPa of pressure followed by peak metamorphism at 0.9 GPa requires an increase of 0.6 GPa. This indicates a minimum of 20 km of crustal thickening between dyke emplacement and peak metamorphism. A probable mechanism of crustal thickening in this case is thrust imbrication and crustal loading of material from north to south. The structural feature associated with this imbrication is most likely the Ikertôq shear zone (Fig. 1). The imbrication of rock types, the lithostratigraphic changes, including the disappearance of the Kangâmiut dykes, and the lateral continuity of the Ikertôq shear zone suggest that it is a major structure capable of accommodating displacement of material that buried the northern portion of the dyke swarm with 20 km of overburden. Crustal thickening must have occurred over a minimum map distance of 50 km extending from the Ikertôq shear zone to at least the Itivdleq shear zone (Fig. 1) and farther to the south approaching the Nagssugtoqidian front where the last significant metamorphism occurs.

Summary and conclusions

The 2.04 Ga Kangâmiut dyke swarm in West Greenland is composed of tholeiitic dykes that intruded during passive rifting of Archaean continental crust. The current level of exposure corresponds to emplacement depths less than 10 km based on estimated host rock temperatures less than 450°C during emplacement and geothermobarometry for

Kangâmiut dyke clinopyroxenes. Major and trace element systematics show that the parental magmas for the Kangâmiut dykes differentiated by fractionation of plagioclase, clinopyroxene, olivine, and late state Fe-Ti oxides. The rare-earth element systematics of the dykes indicate initiation of mantle melting at *c.* 2.75 GPa, corresponding to a potential mantle temperature of *c.* 1420°C. This temperature is consistent with ambient mantle temperature estimates for 2.0 Ga and shows that the Kangâmiut dyke swarm formed during passive rifting of the Kenorland supercontinent. Anomalously hot plume mantle is not required for their generation. Subsequent metamorphism of the northern portion of the swarm reached granulite facies, with an estimated temperature of 800°C and pressure of 0.9 GPa. The emplacement pressure of less than 0.3 GPa and peak metamorphism at 0.9 GPa indicate a minimum of 20 km of crustal thickening associated with the Nagssugtoqidian orogeny. Crustal thickening likely occurred during thrusting of material from the central Nagssugtoqidian orogen southward over the southern Nagssugtoqidian orogen along the Ikertôq shear zone.

Acknowledgements

We are especially grateful to the late David Bridgwater, whose boundless energy and enthusiasm for the Kangâmiut dykes inspired this work from beginning to end. We also thank Flemming Mengel, Jim Connelly, and Minik Rosing for their support of this project at various stages, and Andy Saunders and Karen Hanghøj for their constructive reviews of the final manuscript. This work was partially supported by the Danish Lithosphere Centre and grants from the US National Science Foundation (EAR 97-06677 and OCE 98-11453).

References

Abbott, D., Burgess, L., Longhi, J. & Smith, W.H.F. 1994: An empirical thermal history of the Earth's upper mantle. Journal of Geophysical Research 99(7), 13835–13850.

Arculus, R.J. 1994: Aspects of magma genesis in arcs. Lithos 33(1–3), 189–208.

Aspler, L.B. & Chiarenzelli, J.R. 1998: Two Neoarchean supercontinents? Evidence from the Paleoproterozoic. Sedimentary Geology 120(1–4), 75–104.

Bacon, C.R., Bruggman, P.E., Christiansen, R.L., Clynne, M.A., Donnelly-Nolan, J.M. & Hildreth, W. 1997: Primitive magmas at five Cascade volcanic fields; melts from hot, heterogeneous sub-arc mantle. Canadian Mineralogist 35(4), 397–423.

Bailey, J.C., Frolova, T.I. & Burikova, I.A. 1989: Mineralogy, geochemistry and petrogenesis of Kurile island-arc basalts. Contributions to Mineralogy and Petrology 102(3), 265–280.

Bak, J., Korstgård, J. & Sørensen, K. 1975: A major shear zone within the Nagssugtoqidian of West Greenland. Tectonophysics 27(3), 191–209.

Baker, D.R. & Eggler, D.H. 1987: Compositions of anhydrous and hydrous melts coexisting with plagioclase, augite, and olivine or low-Ca pyroxene from 1 atm to 8 kbar; application to the Aleutian volcanic center of Atka. American Mineralogist 72(1–2), 12–28.

Baker, M.B. & Stolper, E.M. 1994: Determining the composition of high-pressure mantle melts using diamond aggregates. Geochimica et Cosmochimica Acta 58(13), 2811–2827.

Becker, H., Jochum, K.P. & Carlson, R.W. 1999: Constraints from high-pressure veins in eclogites on the composition of hydrous fluids in subduction zones. Chemical Geology 160(4), 291–308.

Bell, D.R. & Rossman, G.R. 1992: Water in Earth's mantle; the role of nominally anhydrous minerals. Science 255(5050), 1391–1397.

Berman, R.G. 1991: Thermobarometry using multi-equilibrium calculations; a new technique, with petrological applications. The Canadian Mineralogist 29, 833–855.

Blichert-Toft, J., Rosing, M.T., Lesher, C.E. & Chauvel, C. 1995: Geochemical constraints on the origin of the late Archean Skjoldungen alkaline igneous province, SE Greenland. Journal of Petrology 36(2), 515–561.

Bridgwater, D., Mengel, F., Fryer, B., Wagner, P. & Hansen, S.C. 1995: Early Proterozoic mafic dykes in the North Atlantic and Baltic cratons: field setting and chemistry of distinctive swarms. In: Coward, M.P. & Ries, A.C. (eds): Early Precambrian processes. Geological Society Special Publication (London) 95, 193–220.

Brophy, J.G. & Marsh, B.D. 1986: On the origin of high alumina arc basalt and the mechanics of melt extraction. Journal of Petrology 27(4), 763–789.

Cadman, A.C., Noble, S.R., Tarney, J., Park, G., Ryan, A.B. & Royse, K.R. 1999: U-Pb ages of syndeformational dykes associated with the Mesoproterozoic Nain Plutonic Suite, Labrador. Canadian Journal of Earth Sciences 36(3), 339–348.

Cadman, A.C., Tarney, J., Bridgwater, D., Mengel, F.C., Whitehouse, M.J. & Windley, B.F. 2001: The petrogenesis of the Kangâmiut dyke swarm, W. Greenland. Precambrian Research 105, 183–203.

Carslaw, H.S. & Jaeger, J.C. 1959: Conduction of heat in solids, 510 pp., Oxford: Clarendon Press.

Chen, W. & Molnar, P. 1983: Focal depths of intracontinental and intraplate earthquakes and their implications for the thermal and mechanical properties of the lithosphere. Journal of Geophysical Research 88(5), 4183–4214.

Connelly, J.N. & Mengel, F.C. 2000: Evolution of Archean components in the Paleoproterozoic Nagssugtoqidian orogen, West Greenland. Geological Society of America Bulletin 112(5), 747–763.

Connelly, J.N., van Gool, J.A.M. & Mengel, F.C. 2000: Temporal evolution of a deeply eroded orogen: the Nagssugtoqidian Orogen, West Greenland. Canadian Journal of Earth Sciences 37, 1121–1142.

Danyuschevsky, L.V., Eggins, S.M., Falloon, T.J. & Christie, D.M. 2000: H_2O abundance in depleted to moderately enriched mid-ocean ridge magmas; Part 1: Incompatible behavior, implications for mantle stor-

age, and origin of regional variations. Journal of Petrology 41, 1329–1364.

Escher, A. & Pulvertaft, T.C.R. 1976: Rinkian mobile belt of West Greenland. In: Escher A. and Watt W.S. (eds): Geology of Greenland, 104–119. Copenhagen: Geological Survey of Greenland.

Escher, A., Escher, J.C. & Watterson, J. 1975: The reorientation of the Kangâmiut dike swarm, West Greenland. Canadian Journal of Earth Sciences 12, 158–173.

Escher, A., Jack, S. & Watterson, J. 1976: Tectonics of the North Atlantic Proterozoic dyke swarm. Philosophical Transactions of the Royal Society of London, Series A: Mathematical and Physical Sciences 280(1298), 529–539.

Fahrig, W.F. & Bridgwater, D. 1976: Late Archean – early Proterozoic paleomagnetic pole positions from West Greenland. In: Windley, B.F. (ed.): Early history of the Earth, 427–439. New York: John Wiley & Sons.

Fram, M.S. & Lesher, C.E. 1993: Geochemical constraints on mantle melting during creation of the North Atlantic basin. Nature 363, 712–715.

Francalanci, L., Taylor, S.R., McCulloch, M.T. & Woodhead, J.D. 1993: Geochemical and isotopic variations in the calc-alkaline rocks of Aeolian arc, southern Tyrrhenian Sea, Italy; constraints on magma genesis. Contributions to Mineralogy and Petrology 113(3), 300–313.

Friend, C.R.L. & Nutman, A.P. 1994: Two Archaean granulite-facies metamorphic events in the Nuuk–Maniitsoq region, southern West Greenland; correlation with the Saglek Block, Labrador. Journal of the Geological Society (London) 151, 421–424.

Furlong, K.P. & Schwartz, S.Y. 2004: Influence of the Mendocino triple junction on the tectonics of coastal California. Annual Review of Earth and Planetary Sciences 32, 403–433.

Galer, S.J.G. 1991: Interrelationships between continental freeboard, tectonics and mantle temperature. Earth and Planetary Science Letters 105(1–3), 214–228.

Green, T.H. 1994: Experimental studies of trace-element partitioning applicable to igneous petrogenesis; Sedona 16 years later. Chemical Geology 117(1–4), 1–36.

Gribble, R.F., Stern, R.J., Newman, S., Bloomer, S.H. & O'Hearn, T. 1998: Chemical and isotopic composition of lavas from the northern Mariana Trough; implications for magmagenesis in back-arc basins. Journal of Petrology 39(1), 125–154.

Grocott, J. 1979: Shape fabrics and superimposed simple shear strain in a Precambrian shear belt, West Greenland. Journal of the Geological Society (London) 136(7), 471–489.

Gust, D.A., Arculus, R.J. & Kersting, A.B. 1997: Aspects of magma sources and processes in the Honshu Arc. Canadian Mineralogist 35(4), 347–365.

Hageskov, B. 1995: Structural evolution of the southern Nagssugtoqidian front and the role of the Kangâmiut dykes. Terra Nova 7, 107 only.

Hanmer, S., Mengel, F., Connelly, J. & van Gool, J. 1997: Significance of crustal-scale shear zones and synkinematic mafic dykes in the Nagssugtoqidian Orogen, SW Greenland; a re-examination. Journal of Structural Geology 19(1), 59–75.

Harrison, T.M. 1981: Diffusion of ^{40}Ar in hornblende. Contributions to Mineralogy and Petrology 78(3), 324–331.

Hirschmann, M.M. 2000: Mantle solidus: experimental constraints and the effects of peridotite composition. Geochemistry, Geophysics, Geosystems 1(10) (http://dx.doi.org/10.1029/2000GC000070).

Holdaway, M.J. 1971: Stability of andalusite and the aluminum silicate phase diagram. American Journal of Science 271(2), 97–131.

Hooper, P.R. & Hawkesworth, C.J. 1993: Isotopic and geochemical constraints on the origin and evolution of the Columbia River Basalt. Journal of Petrology 34(6), 1203–1246.

Jakes, P. & Gill, J. 1970: Rare earth elements and the island arc tholeiitic series. Earth and Planetary Science Letters 9(1), 17–28.

Jenner, G.A., Longerich, H.P., Jackson, S.E. & Fryer, B.J. 1990: ICP-MS; a powerful tool for high-precision trace-element analysis in earth sciences; evidence from analysis of selected U.S.G.S. reference samples. Chemical Geology 83(1–2), 133–148.

Kalsbeek, F. & Manatschal, G. 1999: Geochemistry and tectonic significance of peridotitic and metakomatiitic rocks from the Ussuit area, Nagssugtoqidian Orogen, West Greenland. Precambrian Research 94, 101–120.

Kalsbeek, F. & Nutman, A.P. 1996: Anatomy of the early Proterozoic Nagssugtoqidian Orogen, West Greenland, explored by reconnaissance SHRIMP U-Pb zircon dating. Geology 24(6), 515–518.

Kalsbeek, F., Pidgeon, R.T. & Taylor, P.N. 1987: Nagssugtoqidian mobile belt of West Greenland; a cryptic 1850 Ma suture between two Archaean continents; chemical and isotopic evidence. Earth and Planetary Science Letters 85(4), 365–385.

Kelemen, P.B., Hanghøj, K. & Greene, A.R. 2003: One view of the geochemistry of subduction-related magmatic arcs, with an emphasis on primitive andesite and lower crust. In: Rudnick, R.L., Holland, H.D. & Turekian, K.K. (eds): Treatise on Geochemistry: the Crust 3, 593–659.

Korstgård, J.A. 1979: Metamorphism of the Kangâmiut dykes and the metamorphic and structural evolution of the southern Nagssugtoqidian boundary in the Itvidleq–Ikertôq region, West Greenland. Rapport Grønlands Geologiske Undersøgelse 89, 63–75.

Kystol, J. & Larsen, L.M. 1999: Analytical procedures in the Rock Geochemical Laboratory of the Geological Survey of Denmark and Greenland. Geology of Greenland Survey Bulletin 184, 59–62.

Langmuir, C.H., Klein, E.M. & Plank, T. 1992: Petrological systematics of mid-ocean ridge basalts: constraints on melt generation beneath ocean ridges. In: Morgan, J.P., Blackman, D.K. & Sinton, J.M. (eds): Mantle flow and melt generation at mid-ocean ridges. Geophysical Monograph 71, 183–280. Washington D.C.: American Geophysical Union.

Le Maitre, R.W. 2002: A classification of igneous rocks and glossary of terms, 2nd edition., 236 pp. Cambridge: Cambridge University Press.

Leake, B.E. *et al.* 1997: Nomenclature of amphiboles; report of the Subcommittee on Amphiboles of the International Mineralogical Association, Commission on New Minerals and Mineral Names. American Mineralogist 82(9–10), 1019–1037.

Lightfoot, P.C., Hawkesworth, C.J., Hergt, J., Naldrett, A.J., Gorbachev, N.S., Fedorenko, V.A. & Doherty, W. 1993: Remobilisation of the continental lithosphere by a mantle plume; major-, trace-element, and Sr-, Nd-, and Pb-isotope evidence from picritic and tholeiitic

lavas of the Noril'sk District, Siberian Trap, Russia. Contributions to Mineralogy and Petrology 114(2), 171–188.

Manatschal, G., Ulfbeck, D. & van Gool, J. 1998: Change from thrusting to syncollisional extension at a mid-crustal level; an example from the Palaeoproterozoic Nagssugtoqidian Orogen, West Greenland. Canadian Journal of Earth Sciences 35(7), 802–819.

Mayborn, K.R. 2000: Petrogenesis of the Paleoproterozoic Kangâmiut dike swarm, West Greenland: implications for the tectonic history of northeast Laurentia and the evolution of basaltic magmas, 318 pp. Unpublished Ph.D. thesis, University of California-Davis, USA.

Mayborn, K.R. & Lesher, C.E. 2004: Paleoproterozoic mafic dike swarms of northeast Laurentia: products of plumes or ambient mantle? Earth and Planetary Science Letters 225(3), 305–317.

Mengel, F., van Gool, J. & Marker, M. 1995: Mafic dykes as monitors of orogenic development: an example from the southern margin of the Palaeoproterozoic Nagssugtoqidian Orogen, West Greenland. Proceedings, First DLC Workshop on the Nagssugtoqidian Orogen in West Greenland, 6–7 April, 15–18. Copenhagen, Denmark: Danish Lithosphere Centre.

Mengel, F., Bridgwater, D. & Hageskov, B. 1996: Southern Nagssugtoqidian foreland: tectonic and thermal evolution monitored by the Proterozoic Kangâmiut dyke swarm. LITHOPROBE Report 57, 177–191.

Miller, D.M., Goldstein, S.L. & Langmuir, C.H. 1994: Cerium/lead and lead isotope ratios in arc magmas and the enrichment of lead in the continents. Nature 368(6471), 514–520.

Noe-Nygaard, A. 1952: A new orogenic epoch in the pre-Cambrian of Greenland. International Geological Congress, Part 13(59), 199–204. International Geological Congress.

Nutman, A.P. & Bridgwater, D. 1986: Early Archaean Amitsop tonalites and granites of the Isukasia area, southern West Greenland; development of the oldest-known sial. Contributions to Mineralogy and Petrology 94(2), 137–148.

Nutman, A.P. & Collerson, K.D. 1991: Very early Archean crustal-accretion complexes preserved in the North Atlantic Craton. Geology 19(8), 791–794.

Nutman, A.P., Kalsbeek, F., Marker, M., van Gool, J. & Bridgwater, D. 1999: U-Pb zircon ages of Kangâmiut dykes and detrital zircons in metasediments in the Palaeoproterozoic Nagssugtoqidian Orogen (West Greenland); clues to the pre-collisional history of the orogen. Precambrian Research 93(1), 87–104.

Papike, J.J., Cameron, K.L. & Baldwin, K. 1974: Amphiboles and pyroxenes; characterization of other than quadrilateral components and estimates of ferric iron from microprobe data. Abstracts with Programs – Geological Society of America 6, 1053–1054.

Pearce, J.A., Baker, P.E., Harvey, P.K. & Luff, I.W. 1995: Geochemical evidence for subduction fluxes, mantle melting and fractional crystallization beneath the South Sandwich island arc. Journal of Petrology 36(4), 1073–1109.

Peate, D.W. & Hawkesworth, C.J. 1996: Lithospheric to asthenospheric transition in low-Ti flood basalts from southern Parana, Brazil. Chemical Geology 127, 1–24.

Perfit, M.R., Gust, D.A., Bence, A.E., Arculus, R.J. & Taylor, S.R. 1980: Chemical characteristics of island-arc basalts; implications for mantle sources. Chemical Geology 30(3), 227–256.

Plank, T. & Langmuir, C.H. 1988: An evaluation of the global variations in the major element chemistry of arc basalts. Earth and Planetary Science Letters 90(4), 349–370.

Plank, T. & Langmuir, C.H. 1992: Effects of the melting regime on the composition of the oceanic crust. Journal of Geophysical Research 97(13), 19749–19770.

Putirka, K., Kinzler, R., Longhi, R. & Walker, D. 1996: Thermobarometry of mafic igneous rocks based on clinopyroxene-liquid equilibria, 0–30 kbar. Contributions to Mineralogy and Petrology 123(1), 92–108.

Ramberg, H. 1949: On the petrogenesis of the gneiss complexes between Sukkertoppen and Christianshaab, West-Greenland. Meddelelser fra Dansk Geologisk Forening 11, 312–327.

Reay, A. & Harris, B. 1964: The partial fusion of peridotite. Bulletin of Volcanology 27, 115–127.

Reches, Z. & Fink, J. 1988: The mechanism of intrusion of the Inyo Dike, Long Valley Caldera, California. Journal of Geophysical Research 93(5), 4321–4334.

Richter, F.M. 1984: Regionalized models for the thermal evolution of the Earth. Earth and Planetary Science Letters 68(3), 471–484.

Roeder, P.L. & Emslie, R.F. 1970: Olivine-liquid equilibrium. Contributions to Mineralogy and Petrology 29(4), 276–289.

Spear, F.S. 1981: An experimental study of hornblende stability and compositional variability in amphibole. American Journal of Science 281(6), 697–734.

Stein, C.A. 1995: Heat flow of the Earth. In: Ahrens, T.J. (ed.): Global earth physics: a handbook of physical constants, 144–158. Washington D.C.: American Geophysical Union.

Stern, R.A., Percival, J.A. & Mortensen, J.K. 1994: Geochemical evolution of the Minto Block; a 2.7 Ga continental magmatic arc built on the Superior proto-craton. Precambrian Research 65(1–4), 115–153.

Storey, M., Mahoney, J.J. & Saunders, A.D. 1997: Cretaceous basalts in Madagascar and the transition between plume and continental lithosphere mantle sources. In: Mahoney, J.J. & Coffin, M.F. (eds): Large igneous provinces; continental, oceanic, and planetary flood volcanism, 95–122. Washington D.C.: American Geophysical Union.

Sun, S.S. & McDonough, W.F. 1989: Chemical and isotopic systematics of oceanic basalts; implications for mantle composition and processes. In: Saunders, A.D. & Norry, M. J. (eds): Magmatism in the ocean basins. Geological Society Special Publication (London) 42, 313–345.

Takahashi, E. 1986: Melting of a dry peridotite KLB-1 up to 14 GPa; implications on the origin of peridotitic upper mantle. Journal of Geophysical Research 91(9), 9367–9382.

Tatsumi, Y. 1989: Migration of fluid phases and genesis of basalt magmas in subduction zones. Journal of Geophysical Research 94(4), 4697–4707.

Tatsumi, Y., Otofuji, Y., Matsuda, T. & Nohda, S. 1989: Opening of the Sea of Japan back-arc basin by asthenospheric injection. Tectonophysics 166(4), 317–329.

Thompson, R.N. 1982: Magmatism of the British Tertiary volcanic province. Scottish Journal of Geology 18, 49–107.

Tormey, D.R., Grove, T.L. & Bryan, W.B. 1987: Experimental petrol-

ogy of normal MORB near the Kane fracture zone; 22 degree–25 degree N, Mid-Atlantic Ridge. Contributions to Mineralogy and Petrology 96(2), 121–139.

Tormey, D.R., Hickey-Vargas, R., Frey, R.A. & Lopez-Escobar, L. 1991: Recent lavas from the Andean volcanic front (33–42 degrees S); interpretations of along-arc compositional variations. In: Harmon, R.S. (ed.): Andean magmatism and its tectonic setting. Geological Society of America Special Paper 265, 57–77.

van Gool, J.A.M., Kriegsman, L.M., Marker, M. & Nichols, G.T. 1999: Thrust stacking in the inner Nordre Strømfjord area, West Greenland; significance for the tectonic evolution of the Palaeoproterozoic Nagssugtoqidian Orogen. Precambrian Research 93(1), 71–85.

van Gool, J.A.M., Connelly, J.N., Marker, M. & Mengel, F.C. 2002: The Nagssugtoqidian Orogen of West Greenland: tectonic evolution and regional correlations from a West Greenland perspective. Canadian Journal of Earth Sciences 39(5), 665–686.

Williams, C.F. 1996: Temperature and the seismic/aseismic transition; observations from the 1992 Landers earthquake. Geophysical Research Letters 23(16), 2029–2032.

Williams, H., Hoffman, P.F., Lewry, J.F., Monger, J.W.H. & Rivers, T. 1991: Anatomy of North America; thematic geologic portrayals of the continent. Tectonophysics 187(1–3), 117–134.

Willigers, B.J.A., Mengel, F.C., Bridgwater, D., Wijbrans, J.R. & van Gool, J.A.M. 1999: Mafic dike swarms as absolute time markers in high-grade terranes; $^{40}Ar/^{39}Ar$ geochronological constraints on the Kangâmiut dikes, West Greenland. Geology 27(9), 775–778.

Windley, B.F. 1970: Primary quartz ferro-dolerite/garnet amphibolite dykes in the Sukkertoppen region of West Greenland. In: Newall, G. & Rast, N. (eds): Mechanism of igneous intrusion, 79–92. Liverpool: Seel House Press.

Wooden, J.L., Czamanske, G.K., Fedorenko, V.A., Arndt, N.T., Chauvel, C., Bouse, R.M., King, B.W., Knight, R.J. & Siems, D.F. 1993: Isotopic and trace-element constraints on mantle and crustal contributions to Siberian continental flood basalts, Noril'sk area, Siberia. Geochimica et Cosmochimica Acta 57(15), 3677–3704.

Manuscript received 8 June 2004; revision accepted 15 August 2005

Appendix

Table A1. Field data for Kangâmiut dykes examined for this study

Dyke	Location	Latitude	Longitude	Trend	Thickness (m)	Samples
1	Søndre Strømfjord	66°05.266'N	053°33.211'W	010	2	430901 middle of dyke, 430902 near contact
2	Søndre Strømfjord	66°05.26'N	053°33.5'W	080	20	430903 ~7 m from dyke contact
3	Søndre Strømfjord	66°05.26'N	053°33.5'W	010	0.4	none
4	Søndre Strømfjord	66°05.26'N	053°33.7'W	020	?	none
5	Itilleq	66°33.3'N	053°02.5'W	086	6	430904 ~2 m from contact
6	Itilleq	66°33.3'N	053°02.5'W	?	1.5	430905 middle of dyke
7	Ikertooq	66°58.1'N	052°28.9'W	079	0.3	none
8	Ikertooq	66°58.1'N	052°28.9'W	123	0.15	none
9	Ikertooq	66°57.55'N	052°31.7'W	010	2	430910 0.5 m from dyke margin
10	Ikertooq	66°58.95'N	052°26.8'W	080	2	430915 middle of dyke
11	Ikertooq	66°49.7'N	052°16.7'W	054	0.3	430917 middle of dyke
12	Ikertooq	66°50.1'N	052°19.2'W	?	?	430919 middle of dyke
13	Itilleq	66°32.25'N	052°45.0'W	080	8	430923 middle of dyke
14	Itilleq	66°32.85'N	052°47.15'W	?	0.1	430926 whole width of dyke
15	Itilleq	66°33.3'N	052°51.3'W	095	1	430929 middle of dyke
16	Itilleq	66°33.03'N	052°53.54'W	035	8	430930 ~2.5 m from contact, 430931 dyke contact
17	Itilleq	66°33.5'N	052°56.0'W	080	2	430933 0.3 m from contact
18	Itilleq	66°34.7'N	052°56.0'W	062	10	430935 middle of dyke
19	Itilleq	66°34.7'N	052°56.0'W	090	14	430936 middle of dyke
20	Itilleq	66°35.1'N	052°49.0'W	090	8	430939 middle of dyke
21	Itilleq	66°35.1'N	052°47.5'W	079	8	430940 middle of dyke
22	Itilleq	66°34.75'N	052°48.5'W	?	?	430942 middle of dyke
23	Itilleq	66°34.75'N	052°48.5'W	?	?	430943 middle of dyke
24	Itilleq	66°33.1'N	053°04.0'W	?	25	430946 middle of dyke
25	Itilleq	66°33.7'N	052°55.1'W	087	16	430948 middle of dyke, 430950 dyke contact
26	Itilleq	66°33.25'N	052°38.5'W	100	1	430951 middle of dyke
27	Itilleq	66°33.25'N	052°33.0'W	096	20	430952 middle of dyke
28	Itilleq	66°32.6'N	052°27.0'W	057	30	430953 middle of dyke
29	Itilleq	66°31.8'N	052°41.0'W	061	5	430955 ~1.5 m from contact, 430956 ~5 m from contact
30	Itilleq	66°31.9'N	052°38.5'W	085	15	430957 dyke contact, 430959 ~5 m from contact
31	Itilleq	66°31.8'N	052°36.2'W	065	18	430960 middle of dyke
32	Itilleq	66°31.7'N	052°34.0'W	078	22	430961 middle of dyke
33	Mouth of Itilleq	66°29.9'N	053°33.5'W	022	20	430965 middle of dyke
34	Mouth of Itilleq	66°30'N	053°34.8'W	065	25	430966 ~7 m from contact
35	Mouth of Itilleq	66°30.05'N	053°35.8'W	117	40	430967 ~7 m from contact
36	Mouth of Itilleq	66°30.5'N	053°36.4'W	006	10	430969 middle of dyke
37	South of Maniitsoq	65°22.7'N	052°47.3'W	345	4.5	430970 middle of dyke
38	East of Maniitsoq	65°25.5'N	052°24.0'W	?	15	430972 middle of dyke
39	East of Maniitsoq	65°25.4'N	052°23.0'W	054	0.4	430973 middle of dyke
40	East of Maniitsoq	65°25.5'N	052°18.0'W	117	12	430974 middle of dyke
41	East of Maniitsoq	65°26.0'N	052°14.8'W	354	7	430975 middle of dyke
42	East of Maniitsoq	65°35.15'N	052°46.0'W	002	49	430977 dyke contact, 430979 1 m from contact, 430981 5 m from contact, 430982 17 m from contact
43	North of Maniitsoq	65°39.85'N	052°37.0'W	003	25	430983 middle of dyke, 430984 dyke contact
44	North of Maniitsoq	65°44.4'N	052°38.5'W	344	0.5	430986 middle of dyke
45	North of Maniitsoq	65°38.75'N	052°37.5'W	002	16	430987 middle of dyke, 430988 ~6 cm from contact
46	North of Maniitsoq	65°36.9'N	052°43.5'W	005	10	430990 ~4 m from contact, 430991 ~0.5 m from contact

Table A1 *(continued)*

Dyke	Location	Latitude	Longitude	Trend	Thickness (m)	Samples
47	North of Maniitsoq	65°40.1'N	052°49.0'W	010	17	430992 middle of dyke
48	North-east of Kangaamiut	65°54.9'N	053°14.5'W	050	12	430993 ~2 m from contact
49	North-east of Kangaamiut	65°53.95'N	053°16.0'W	045	27	430994 middle of dyke
50	North-east of Kangaamiut	65°53.4'N	053°14.95'W	033	1	none
51	North-east of Kangaamiut	65°53.4'N	053°14.95'W	110	0.2	none
52	North-east of Kangaamiut	65°53.4'N	053°14.95'W	030	1.5	430995 middle of dyke
53	North-east of Kangaamiut	65°53.4'N	053°14.95'W	110	2	430996 middle of dyke
54	North-east of Kangaamiut	65°52.6'N	053°14.0'W	063	60	430997 andesitic portion of dyke, 430998 mafic portion of dyke
55	North-east of Kangaamiut	65°50.8'N	053°13.0'W	064	1.5	432101 middle of dyke
56	North-east of Kangaamiut	65°50.8'N	053°13.0'W	015	15	430999 middle of dyke
57	Søndre Strømfjord	66°01.4'N	053°28.65'W	028	60	432103 middle of dyke
58	Kangerluarsussuaq	66°17.5'N	053°05.65'W	065	40	432104 dyke contact, 432105 middle of dyke
59	Kangerluarsussuaq	66°17.5'N	053°05.8'W	057	40	432107 middle of dyke
60	Kangerluarsussuaq	66°17.25'N	053°07.5'W	022	1	432108 middle of dyke
61	Kangerluarsussuaq	66°17.25'N	053°07.5'W	145	45	432106 1 m from contact, 432108 middle of dyke
62	Kangerluarsussuaq	66°17.15'N	053°08.5'W	045	21	432111 middle of dyke
63	Kangerluarsussuaq	66°17.05'N	053°11.25'W	028	40	432112 ~7 m from contact
64	Kangerluarsussuaq	66°16.9'N	053°09.7'W	031	140	432115 dyke contact, 432116 ~2.5 m from W contact, 432118 ~45 m from W contact, 432119 ~70 m from W contact, 432120 ~95 m from W contact, 432121 ~19 m from E contact, 432122 ~18 m from W contact, 432136 ~40 m from W contact, 432137 middle of dyke
65	Kangerluarsussuaq	66°39.5'N	053°03.0'W	065	50	432123 middle of dyke
66	East of Itilleq	66°29.3'N	052°25.0'W	065	15	432125 middle of dyke
67	East of Itilleq	66°29.1'N	052°24.0'W	050	8	432128 middle of dyke
68	East of Itilleq	66°33.1'N	052°07.5'W	072	1	432129 middle of dyke
69	East of Itilleq	66°31.75'N	052°18.0'W	050	4	432130 middle of dyke
70	East of Itilleq	66°30.5'N	052°27.5'W	090	25	432138 middle of dyke
71	East of Itilleq	66°27.9'N	052°27.0'W	022	70	432133 middle of dyke
72	East of Itilleq	66°26.0'N	052°40.5'W	080	5	432134 middle of dyke
73	East of Itilleq	66°27.45'N	052°45.5'W	055	4	432135 middle of dyke
74	Kangerluarsussuaq	66°16.6'N	053°17.0'W	032	17	432139 middle of dyke
75	Kangerluarsussuaq	66°15.3'N	053°22.5'W	036	18	432140 middle of dyke, 432151 9 m from N contact, 432152 6 m from N contact, 432153 4 m from N contact, 432154 2 m from N contact, 432155 1 m from N contact, 432156 0.5 m from N contact, 432157 0.25 m from N contact, 432158 dyke contact, highly jointed
76	Kangerluarsussuaq	66°14.6'N	053°33.0'W	020	25	432143 middle of dyke, 432144 5 m from E contact, 432145 E contact
77	Kangerluarsussuaq	66°14.7'N	053°31.7'W	044	0.4	432147 NW contact, 432148 middle of dyke 432149 SE contact
78	Kangerluarsussuaq	66°15.15'N	053°29.0'W	086	2	432150 middle of dyke
79	Mouth of Itilleq	66°30.05'N	053°35.8'W	090	50	430206 and 430207 middle of dyke
80	Mouth of Itilleq	66°30.05'N	053°35.8'W	090	15	430208 and 430209 middle of dyke
81	Mouth of Itilleq	66°30.05'N	053°35.8'W	090	?	430210 middle of dyke
82	Mouth of Itilleq	66°30.05'N	053°35.8'W	090	0.1	430211 whole width of dyke
83	Søndre Strømfjord	66°01.4'N	053°28.65'W	?	?	430258 dyke contact
84	North-east of Kangaamiut	65°52.6'N	053°14.9'W	022	30	430267 dyke contact, 430265 middle of dyke
85	North-east of Kangaamiut	65°53.6'N	053°14.9'W	045	30	430283 dyke contact, 430284 middle of dyke
86	North-west of Kangaamiut	65°56.6'N	053°28.0'W	25	60	158074 and 430288 dyke contact, 432102 and 158077 middle of dyke

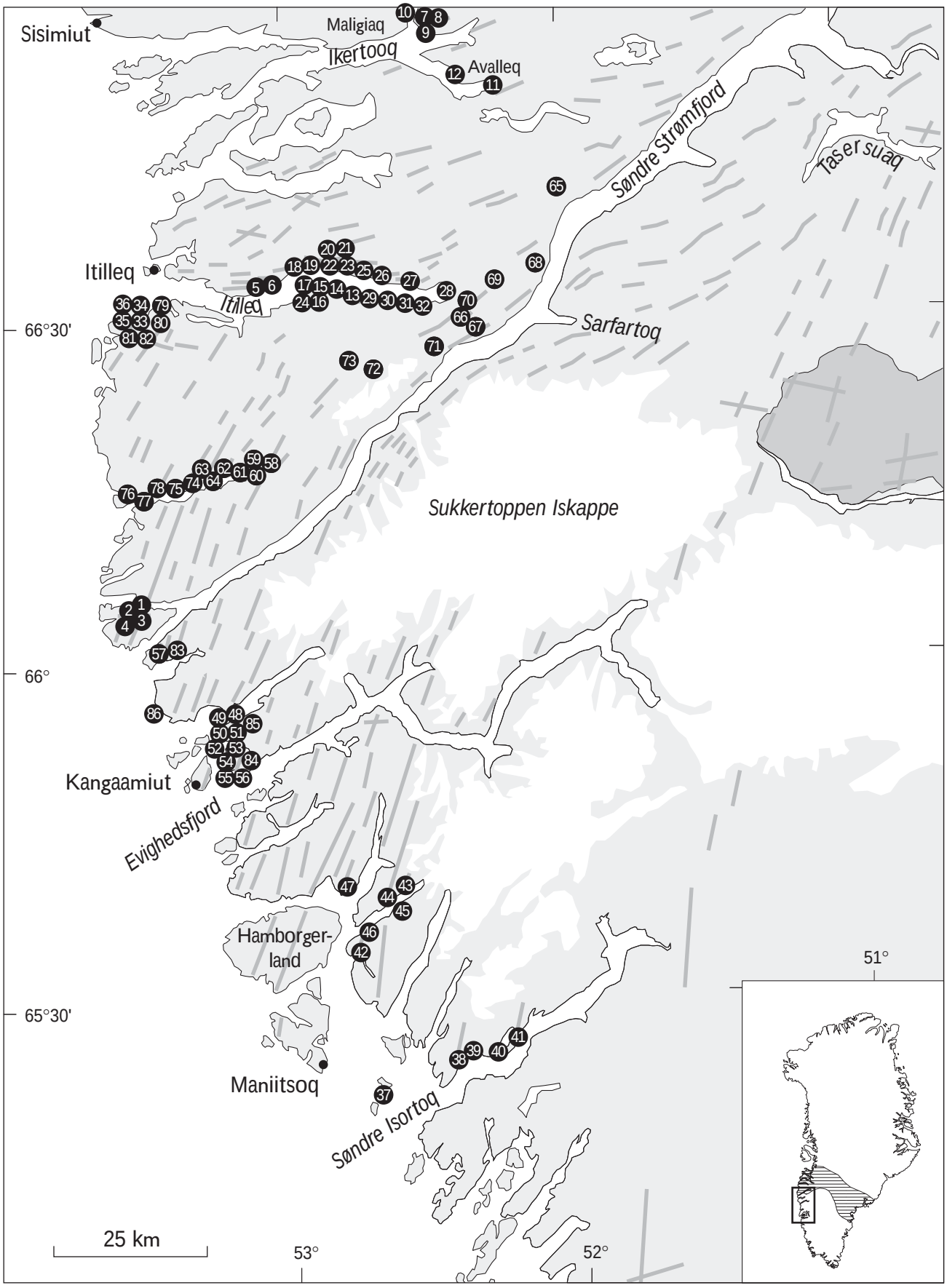

Fig. A1. Map showing the locations of dykes examined in this study.